Influence of convective processes on the isotopic composition (δ^{18}O and δD) of precipitation and water vapor in the tropics: 1. Radiative-convective equilibrium and Tropical Ocean–Global Atmosphere–Coupled Ocean-Atmosphere Response Experiment (TOGA-COARE) simulations

Sandrine Bony,[1] Camille Risi,[1] and Françoise Vimeux[2]

Received 8 February 2008; revised 18 May 2008; accepted 4 August 2008; published 11 October 2008.

[1] Cumulus convection constitutes a key process in the control of tropical precipitation and the vertical transport of atmospheric water. To better understand the influence of convective processes on the isotopic composition of precipitation and water vapor, water stable isotopes ($H_2^{18}O$ and HDO) are introduced into a single column model including the Emanuel convective parameterization. This paper analyzes unidimensional simulations of the tropical atmosphere in a state of radiative-convective equilibrium, and simulations forced by data from the Tropical Ocean–Global Atmosphere–Coupled Ocean-Atmosphere Response Experiment (TOGA-COARE). This study shows that deep convective atmospheres are associated with robust isotopic features such as an isotopic composition of the air below the tropical tropopause layer (around 12–13 km) close to the typical values observed in the lower tropical stratosphere, and an isotopic enrichment of the upper tropospheric water that starts well below the tropopause. It highlights the critical role of condensate lofting and convective detrainment in these features, and the role of convective unsaturated downdrafts in the control of the isotopic composition of precipitation. Finally, it shows that the so-called ''amount effect'' primarily reveals the influence of large-scale atmospheric circulation changes on the isotopic composition of the precipitation, and that temperature changes not associated with circulation changes lead to an ''anti–amount effect''. The detailed analysis of the physical processes underlying the ''amount effect'' is presented in a companion paper.

Citation: Bony, S., C. Risi, and F. Vimeux (2008), Influence of convective processes on the isotopic composition (δ^{18}O and δD) of precipitation and water vapor in the tropics: 1. Radiative-convective equilibrium and Tropical Ocean–Global Atmosphere–Coupled Ocean-Atmosphere Response Experiment (TOGA-COARE) simulations, *J. Geophys. Res.*, *113*, D19305, doi:10.1029/2008JD009942.

1. Introduction

[2] Water molecules exist under various isotopic forms in the ocean and in the atmosphere. Owing to mass and symmetry differences, the different stable forms of the water molecule ($H_2^{16}O$, HDO, $H_2^{18}O$) have slightly different physical properties (saturation vapor pressure, molecular diffusivity), and are thus redistributed between the vapor and condensed phases at each phase change. This redistribution is named ''isotopic fractionation''. As it depends on the physical conditions in which it occurs, the ratio of heavy and light isotopes in water constitutes a potential tracer of the hydrologic cycle and of past climate variations.

[3] Isotopic records from polar ice cores have long been used to reconstruct paleotemperature variations at high latitudes [*Jouzel*, 2003]. At low latitudes on the other hand, the reconstitution of past climate variations is hampered by our difficulty to interpret quantitatively the isotopic variations inferred from tropical ice cores. Indeed, observed variations of the isotopic composition of the water precipitated over the South American Andes and stored in mountain glaciers have been interpreted either in terms of relative humidity variations [*Broecker*, 1997], runoff variations [*Pierrehumbert*, 1999], local variations of the temperature of condensation [*Thompson et al.*, 2000], or remote precipitation variations [*Ramirez et al.*, 2003; *Hoffmann et al.*, 2003].

[1] Laboratoire de Météorologie Dynamique, IPSL, UPMC, CNRS, Paris, France.
[2] IRD-UR Great Ice, LSCE, IPSL, CEA, UVSQ, CNRS, Gif-sur-Yvette, France.

0148-0227/08/2008JD009942

[4] This difficulty results in part from our limited understanding of the physical processes that control the tropical isotope behavior, and from the large number of factors potentially affecting the isotopic composition of tropical precipitation. Among those factors are the local precipitation amount [*Dansgaard*, 1964; *Rozanski et al.*, 1993], the precipitation amount all along the air parcels' trajectories [*Vuille et al.*, 2003; *Vimeux et al.*, 2005], the moisture source of the precipitation [*Cole et al.*, 1999], the recycling of water through land-surface exchange processes [*Gat and Matsui*, 1991; *Pierrehumbert*, 1999; *McGuffie and Henderson-Sellers*, 2004] or through precipitation reevaporation in unsaturated air [*Worden et al.*, 2007], and the degree of organization of convective systems [*Lawrence et al.*, 2004]. Many of these factors are related to atmospheric convection, which is a key process in the control of tropical precipitation and in the moistening of the tropical atmosphere [e.g., *Emanuel and Zivkovic-Rothman*, 1999; *Garreaud*, 2000].

[5] Atmospheric convection is also responsible for much of the vertical water transport in the tropics. In the vicinity of the tropopause, however, it is not yet firmly established whether the transport of water from the upper troposphere to the lower stratosphere is accomplished through convective or nonconvective processes, and how the air is dehydrated during this transport [*Rosenlof*, 2003; *Küpper et al.*, 2004]. The signature of convective processes on the isotopic composition of water in the tropical transition layer has been proposed as a possible way to discriminate between the different transport scenarios [*Moyer et al.*, 1996; *Rosenlof*, 2003; *Webster and Heymsfield*, 2003; *Smith et al.*, 2006; *Hanisco et al.*, 2007].

[6] Understanding and quantifying how convection affects the isotopic composition of atmospheric water and precipitation would thus help to better interpret the isotopic measurements made in the tropics, and to relate them more readily to specific atmospheric processes or climate variations.

[7] The isotopic composition of water, just as the humidity distribution, depends on how water is transported, condensed, precipitated and reevaporated. Observations indicate that in convective systems, the transport of air is accomplished episodically and inhomogeneously through an ensemble of updrafts and downdrafts that detrain at multiple altitudes, depending on their entrainment of dry environmental air (see *Emanuel* [1991] for an extended discussion of this matter). The isotopic composition of the vapor or condensed water transported by each updraft depends on the initial composition (and thus the origin) of the rising parcel, and on the fraction of water that condenses during the ascent. The composition of the total (vapor plus condensed) water depends in addition on microphysical processes that determine the fraction of condensed water that is converted to precipitation (and thus how much condensed water remains in the detraining air). The isotopic composition of the precipitation at any vertical level depends on the composition of the water falling from above, on the fraction of the precipitation that is reevaporated in unsaturated air, and on isotopic exchanges that take place between the falling drops and the vapor surrounding them. The influence of convection on the water isotopic composition depends therefore sensitively on a large combination of physical, microphysical and turbulent processes occurring within clouds.

[8] Many modeling studies have been carried out to study the processes that control the isotopes distribution in climate. Some have been using simple conceptual or analytic models to focus on some individual process [e.g., *Pierrehumbert*, 1999], while others have been using complex general circulation models (GCMs) to take into account most of the dynamical and physical mechanisms potentially involved in the global isotope cycle [*Hoffmann et al.*, 1998; *Mathieu et al.*, 2002; *Noone and Simmonds*, 2002; *Schmidt et al.*, 2005; *Vuille and Werner*, 2005]. Other studies focusing on the isotopic composition of the tropical tropopause transition layer (TTL) have used conceptual models [e.g., *Keith*, 2000; *Johnson et al.*, 2001; *Dessler and Sherwood*, 2003] or Lagrangian trajectory models complemented with a simple representation of cloud microphysics and an implicit or idealized representation of convective processes [e.g., *Gettelman and Webster*, 2005; *Dessler et al.*, 2007].

[9] In this study, we introduce water stable isotopes ($H_2^{18}O$ and HDO) and a representation of isotopic fractionation processes [*Hoffmann et al.*, 1998; *Schmidt et al.*, 2005] into a single-column model (SCM) whose physics package incorporates the essential physics that controls tropical atmospheric water and precipitation [*Emanuel and Zivkovic-Rothman*, 1999], and that has been carefully evaluated against tropical data [*Bony and Emanuel*, 2001]. The use of a SCM precludes any claim that we are representing all the complexity of the tropical isotope behavior. Our goal here is rather to understand the role of a few physical processes in the convective control of the water isotopic composition within a deliberately simple framework.

[10] The model used in the present study (the physics package and its isotope module) is presented in section 2. In section 3, we assess the ability of the model to simulate the isotopic composition of surface precipitation by forcing the model by large-scale meteorological reanalyses over several tropical marine stations where monthly isotopic data are available. In section 4, we examine how water isotopes are vertically distributed in an atmosphere in radiative-convective equilibrium, and we investigate how the isotopic composition of atmospheric water and precipitation depends on model parameters, and on climate boundary conditions. A physical interpretation of the amount effect based on these simulations is presented in a companion paper [*Risi et al.*, 2008]. In section 5, we force the SCM by large-scale advections of heat and moisture derived from the TOGA COARE experiment to examine how the isotopic compositions of water vapor and precipitation evolve under a time-varying, observed forcing over a region associated with a strong intraseasonal variability of deep convection. A conclusion and a discussion are presented in section 6.

2. Model and Experiments

2.1. Convection and Cloud Parameterizations

[11] The representation of convection used in the model is based on the convection scheme originally developed by *Emanuel* [1991] and subsequently revised and optimized in its prediction of humidity by *Emanuel and Zivkovic-Rothman* [1999]. It is based on the premise that the essential physics that controls atmospheric water vapor include turbulent entrainment, cloud microphysical processes, and

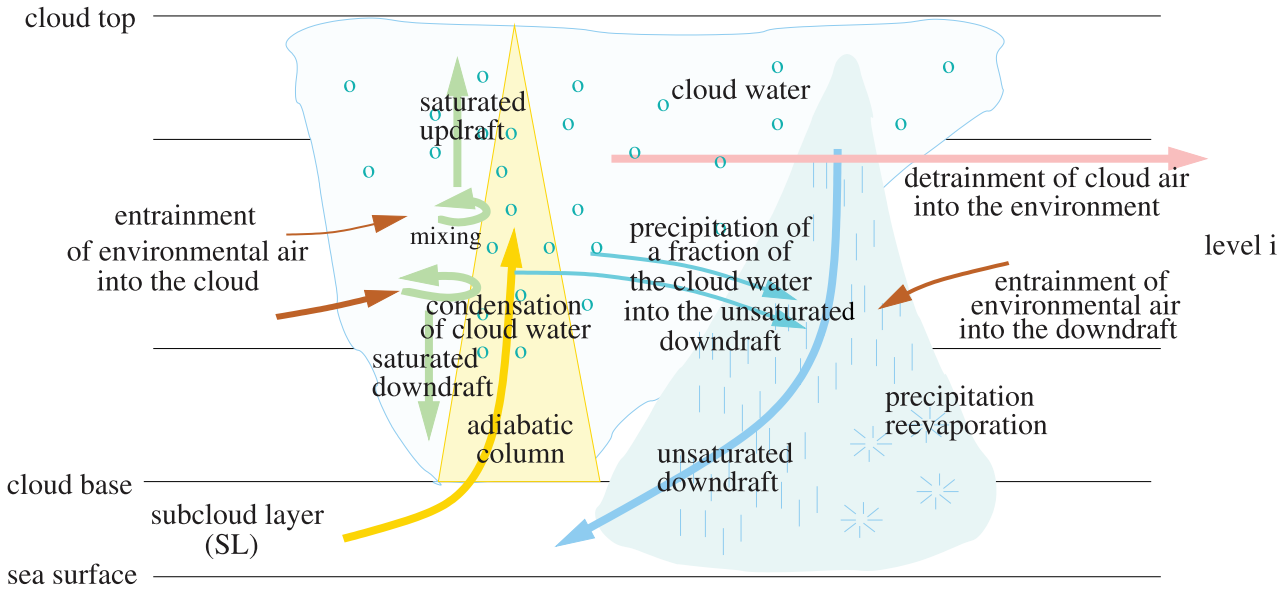

Figure 1. Schematic picture illustrating the representation of convection in the Emanuel scheme.

unsaturated downdrafts driven by the evaporation of the falling precipitation (Figure 1).

[12] Unstable air parcels are first lifted adiabatically (i.e., without mixing) from the subcloud layer (hereafter referred to as SL) to each level i between cloud base and cloud top (the level of neutral buoyancy or the level of zero convective available potential energy (CAPE), to allow for the occurrence of convective overshoot). A fraction $\epsilon_p(i)$ of the condensed water formed between cloud base and level i (the cloud water in excess of a temperature-dependent threshold q_l) is converted to precipitation, while the remaining air is mixed with the unperturbed environment (we call "environment" the air outside the convective drafts): $\epsilon_p = \epsilon_p^{\max}\ (1 - \frac{ql}{q_{cloud}})$, with

$$q_l = \begin{cases} e_{crit} & T \geq 0^o C \\ e_{crit}\left(1 - \frac{T}{T_{crit}}\right) & T_{crit} < T < 0^o C \\ 0 & T \leq T_{crit} \end{cases} \quad (1)$$

where q_{cloud} is the in-cloud mixing ratio of condensed water before precipitation in kg/kg and T is the ascending parcel's temperature in degrees C. The values and the meaning of the different coefficients are given in Table 1.

[13] The mixing representation is assumed to be episodic and inhomogeneous: at each level i, the environmental air is mixed into the cloud in various proportions, forming a spectrum of mixtures. Each mixture then ascends or descends according to its buoyancy (in ascending mixture, water may condense further and produce some precipitation), and detrains back to the environment at the level where it is neutrally buoyant after total reevaporation of its condensate. In such a representation, consistent with observations of cumulus clouds [*Raymond and Blyth*, 1986; *Taylor and Baker*, 1991], the air detrained at any particular level thus arises from a large ensemble of drafts, more or less diluted and originating from different levels in the cloud. The precipitation partially or totally reevaporates as it falls through unsaturated atmospheric layers, driving an unsaturated downdraft. The convective mass fluxes are calculated in order to drive the subcloud layer to quasi-equilibrium.

[14] The statistical cloud scheme developed by *Bony and Emanuel* [2001] is used to predict the cloudiness (cloud fraction and water content) associated with cumulus convection.

2.2. Single Column Model

[15] The unidimensional model used in this study is that used (and evaluated) by *Bony and Emanuel* [2001], complemented by an isotope module described below. We use it with a time step of 300 s and a 25 hPa vertical resolution (40 vertical levels). The choice of this resolution was motivated by the studies of *Emanuel and Zivkovic-Rothman*

Table 1. Physical Signification of the Model Parameters Used in Sensitivity Tests

Parameter Name	Description	Control Value
sigs (σ_s)	fraction of the precipitation falling in unsaturated layers	0.12
omtrain	fall speed of rain	50 Pa/s
coeffr	evaporation coefficient for rain	1
omtsnow	fall speed of snow	5.5 Pa/s
coeffs	evaporation coefficient for snow	0.8
sigd (σ_d)	fractional area covered by the unsaturated downdraft	0.05
beta	coupling coefficient between surface fluxes and gust winds generated by unsaturated downdrafts	10
e_{crit}	autoconversion threshold used in the calculation of ϵ_p	0.0011 kg/kg
T_{crit}	critical temperature used in the calculation of ϵ_p	−55°C
e_p^{max}	maximum value of ϵ_p	0.999
λ	isotopic coefficient for kinetic effects during ice condensation	0.002
ϕ	isotopic coefficient for kinetic effects during rain reevaporation	0.9

Table 2. Summary of the Notations Used in Section 2.3 and Their Signification

Notation	Signification
R	isotopic ratio: ratio of heavy water molecules over $H_2^{16}O$ molecules
R_v	isotopic ratio in vapor
R_l	isotopic ratio in liquid condensate
α_{liq}^{eq}	equilibrium fractionation coefficient between liquid and vapor including a kinetic effect due to the condensation in an unsaturated environment
f_v	residual vapor fraction defined as $\frac{q_v}{q_v^0}$ where q_v is the residual vapor mixing ratio and $q_v{}^0$ is the vapor mixing ratio before condensation
R_v^0	isotopic ratio of vapor before condensation
α_{ice}^{eff}	fractionation coefficient between ice and vapor including kinetic effects
S_I	sursaturation with respect to ice
D	diffusivity of $H_2^{16}O$
D_{iso}	diffusivity of the heavy isotope considered (HDO or $H_2^{18}O$)
R_{ice}	isotopic ratio in ice

[1999] and *Tompkins and Emanuel* [2000] showing that such a resolution is necessary for an accurate prediction of the sensitivity of the humidity distribution to cloud microphysics. (Note that as discussed by *Sherwood and Meyer* [2006], the sensitivity of the humidity distribution to cloud microphysics might be stronger in single-column models than in models that include a representation of the large-scale atmospheric circulation.) In addition to the convection and cloud parameterizations presented above, the model includes a radiation parametrization [*Fouquart and Bonnel*, 1980; *Morcrette*, 1991] and computes surface fluxes through bulk aerodynamic formulae. The model is forced at its surface boundary by a prescribed sea surface temperature (SST), a surface albedo and a surface wind speed.

2.3. Implementation of Water Stable Isotopes

[16] In these convection and cloud schemes, water stable isotopes ($H_2^{18}O$, HDO) are treated exactly like "normal water" ($H_2^{16}O$), except that the effect of the isotopic composition of water on air density and large-scale thermodynamics is neglected. Each mixing ratio q of normal water used in the convection scheme has its isotopic counterpart X. Stable water isotopes are transported passively by the different convective updrafts and downdrafts, but they are subject to fractionation whenever a phase change occurs.

[17] Throughout this paper, the deuterium (oxygen 18) isotopic composition will be quantified by the variable δD ($\delta^{18}O$, respectively). The δD (in ‰) is defined as $\delta D = (\frac{R_{sample}}{R_{SMOW}} - 1) \times 1000$, where R_{sample} is the isotopic ratio $\frac{q_{HDO}}{q_{H_2^{16}O}}$ in the analyzed water and R_{SMOW} is the Standard Mean Ocean Water (SMOW) isotopic ratio. A similar definition is used for $\delta^{18}O$. Since the behavior of $\delta^{18}O$ is similar to that of δD at first order, to avoid redundancy we will show results only for δD, but will also analyze the deuterium excess (d), defined as $d = \delta D\text{-}8\delta^{18}O$, which is used as an indicator of the kinetic effects associated with phase changes [*Dansgaard*, 1964].

[18] Equilibrium fractionation coefficients between vapor and liquid water or ice are calculated following *Merlivat and Nief* [1967] and *Majoube* [1971a, 1971b]. Note that laboratory measurements from which these equations were inferred have been performed for temperatures higher than -40°C. Therefore, as pointed out by *Keith* [2000], there might be some uncertainties in the value of these coefficients at colder temperatures, such as those found in the upper troposphere (temperatures as low as -90°C may be simulated around the tropopause).

2.3.1. Condensation in Convective Updrafts

[19] In convective clouds, updrafts are strong enough to carry condensed water upward at a faster rate than the time required (tens of minutes to several hours) for precipitation processes to become efficient [*Houze*, 1981; *Emanuel*, 1997]. Therefore, condensation occurs and cloud grow before precipitation starts to operate. For this reason, in the convection scheme we make the simple assumption that all the condensate formed in the undiluted updraft between the cloud base and any atmospheric level i (or in ascending mixtures as it rises from level j to its detrainment level i) remains inside the parcel until the lifted parcel reaches level i. Only then is a fraction of the total accumulated condensate precipitated.

[20] Virtually all the condensation produced in the model occurs at the subgrid-scale through cumulus convection and is treated as explained above. However, in the rare situations where the large-scale environment is supersaturated, condensation is considered as in situ condensation.

[21] When vapor condensates in the liquid form (at temperature higher than $T_{melt} = 0°C$), isotopic equilibrium is assumed between droplets and the residual vapor. Thus the isotopic ratios in the vapor and liquid phases are respectively given by $R_v = \frac{R_v^0}{\alpha_{liq}^{eq} - fv\left(\alpha_{liq}^{eq} - 1\right)}$ and $R_l = \alpha_{liq}^{eq} R_v$, with notations given in Table 2.

[22] When vapor condensates in the frozen form (at temperatures lower than $T_{ice} = -15°C$), ice crystals are assumed to get isotopically isolated from the residual vapor [*Jouzel and Merlivat*, 1984], and thus a Rayleigh distillation is assumed. In this case the vapor isotopic ratio is given by: $R_v = R_v^0 \cdot (f_v)\alpha_{ice}^{eff-1}$, where α_{ice}^{eff} is the fractionation coefficient between ice and vapor including a kinetic effect when condensation occurs in a supersaturated environment [*Jouzel and Merlivat*, 1984]:

$$\alpha_{ice}^{eff} = \frac{\alpha_{ice}^{eq} S}{1 + \alpha_{ice}^{eq}(S-1)D/D_{iso}}$$

with notations defined in Table 2. The values of the diffusivities D and D_{iso} are derived from *Merlivat* [1978] (diffusivities from *Cappa et al.* [2003] yield similar results for δD, but overestimated values of d). S is parameterized as a function of temperature T as follows: $S = 1 - \lambda T$, where λ is a tunable parameter.

[23] The isotopic ratio in ice is inferred from water mass conservation, since all previously condensed water is conserved:

$$R_{ice} = \frac{R_v^0 - f_v \cdot R_v}{1 - f_v}$$

[24] For the range of temperatures between $T_{melt} = 0°C$ and $T_{ice} = -15°C$, liquid and solid phases are assumed to coexist. The isotopic composition of the total condensate is

Table 3. Summary of the Notations Used in Section 2.3.2 and Their Signification

Notation	Signification
F_X	evaporation flux for isotope X
R_{ocean}	ocean water isotopic ratio
X	mixing ratio of the water isotope X
η	empirical correction factor due to the evaporative enrichment of surface waters
q_{sat}	specific humidity at saturation
ρ_{air}	air density
C_D	surface drag coefficient
V_s	surface wind speed (including both the background mean wind Vs_0 and a gust velocity factor associated with unsaturated downdrafts)
k_{cin}	kinetic factor depending on the surface wind speed [*Merlivat and Jouzel*, 1979]
V_s', X'	terms involved in the influence of unsaturated downdrafts on surface fluxes

then assumed to be a linear combination of the isotopic compositions of the liquid and solid phases.

2.3.2. Precipitation Reevaporation

[25] The precipitation partially reevaporates when it falls through unsaturated air, and the evaporative cooling of air drives an unsaturated downdraft. In the convection scheme, the partial reevaporation of the precipitation generates a single unsaturated downdraft characterized by a mass flux of precipitating water, a water vapor mixing ratio, and two specified parameters (σ_s and σ_d) that represent the fraction of the precipitation shaft that falls through unperturbed environmental air, and the horizontal cross section occupied by the unsaturated downdraft, respectively [*Emanuel*, 1991; *Emanuel and Zivkovic-Rothman*, 1999].

[26] At any vertical level, the isotopic composition of the precipitating water depends on the isotopic composition of the condensed water that has been converted to precipitation at upper levels, on the fraction of it that has reevaporated, and on isotopic exchanges that take place between the falling drops and the downdraft water vapor. The isotopic composition of the downdraft water vapor depends on the amount and the isotopic composition of the environmental air that is entrained dynamically into the downdraft, and on the isotopic exchanges that take place through evaporation and diffusion with the precipitating water.

[27] Since isotopic diffusivities in ice are very low (4 orders of magnitude lower than in liquid water), sublimation of ice is assumed not to fractionate. On the contrary, raindrops reevaporate with fractionation and partially reequilibrate by diffusion with the vapor of the downdraft. The reevaporation and diffusion processes are treated in a unified manner following Stewart's theory [*Stewart*, 1975], as detailed in Appendix A.

[28] The calculation includes kinetic effects associated with reevaporation in an unsaturated environment. For this purpose, the relative humidity at the droplet contact h is parameterized as a function of the relative humidity in the unsaturated downdraft h_b as follows: $h = \phi + (1 - \phi)\, h_b$, where parameter ϕ is used to tune the kinetic effects [*Stewart*, 1975].

2.3.3. Surface Evaporation

[29] Isotopic fractionation is introduced when water is evaporated at the ocean surface (the ocean is considered as an infinite reservoir of water and isotopes). The isotopic evaporation flux associated with isotope X is computed following *Merlivat and Jouzel* [1979] by:

$$F_X = \rho_{air}.C_D.\left\{\overline{|V_s|}\left[\frac{\eta.R_{ocean}.q_{sat}}{\alpha_{liq}^{eq}} - \overline{X(1)}\right] - \overline{V_s'.X'}\right\}(1 - k_{cin})$$

with notations given in Table 3. Note that X' and V_s' refer to the deviations of X and V_s (associated with convective outflows) from their grid-averaged values $\overline{X}$ and $\overline{V_s}$, respectively.

2.4. Experimental Design

[30] Single-column simulations are performed by specifying ocean boundary conditions (surface temperature, surface albedo, surface wind speed) and by imposing a large-scale atmospheric forcing. The atmospheric forcing is derived either from meteorological reanalyses (section 3), from data collected during field experiments (section 5), or from an imposed idealized vertical profile of large-scale vertical velocity ω (section 4). In this later case, we mimic the typical shape of the ω profile in the tropical atmosphere by imposing a vertical profile of ω of cubic shape, with an extremum in the midtroposphere (at 500 hPa) and vanishing values at the surface and at 100 hPa [*Emanuel*, 1991].

[31] Vertical advections of temperature, humidity and water isotopes are computed from the large-scale vertical velocity. The specification of large-scale horizontal advections is less straightforward. In the tropics, neglecting horizontal temperature advections constitutes a good approximation because of the weak horizontal temperature gradients in the free troposphere [*Sobel and Bretherton*, 2000]. On the other hand, horizontal moisture advections constitute a more difficult issue, because there is no established way to specify them in a single column model. Although observations suggest that horizontal advections constitute a non-negligible component of the tropical moisture budget [*Benedict and Randall*, 2007], numerical studies suggest that SCM simulations do not strongly depend on the specification of horizontal moisture advections [*Bergman and Sardeshmukh*, 2004]. (The TOGA-COARE observations used in section 5 suggest that at altitudes below 500 hPa, horizontal advections are three to four times weaker than vertical advections, except during episodes of deepest convection where their magnitude can be half that of vertical advections between 800 and 600 hPa, and equal or exceed that of vertical advections within the planetary boundary layer.) For these reasons, we assume here that the simulated atmospheric column is embedded in a uniform environment and that horizontal advections of humidity and water isotopes ($-\vec{V_H} \cdot \nabla\Phi$, where $\vec{V_H}$ is the horizontal wind and Φ is either q or X) are negligible compared to vertical advections ($-\omega \frac{\partial\Phi}{\partial P}$).

[32] The neglect of horizontal moisture advections is likely to exaggerate the moisture convergence feedback and to overestimate the precipitation variations associated with a given vertical velocity forcing [*Chiang and Sobel*, 2002]. Also, as regions of intense convection surrounded by regions of less intense convection are likely to receive an

Table 4. Name, Location, and Active Years of the Different IAEA Network Stations Used in This Study

Name	Active Years	Ocean Basin	Latitude (deg)	Longitude (deg)
Apia	1962–1977	Pacific	−13.8	−171.8
Barbados	1961–1992	Atlantic	13.0	−59.3
Canton Island	1962–1966	Pacific	−2.77	−171.8
Diego Garcia	1962–1969	Indian	−7.3	72.4
Madang	1968–1882	Pacific	−5.2	139.1
Taguac	1962–1977	Pacific	13.6	144.8
Truk	1968–1977	Pacific	7.5	155.9
Wake Island	1962–1976	Pacific	19.3	166.7
Yap	1968–1976	Pacific	9.5	138.1

inflow of air richer in heavy isotopes than the local air, neglecting horizontal advections of water isotopes may underestimate the isotopic ratio of the air feeding convection. The impact of this approximation will be studied more quantitatively in the future with three-dimensional simulations. In the meantime, the approximation guarantees that the simulated water isotopic composition depends only on local convective processes, which helps one to understand how convective processes affect tropical water isotopes.

[33] The radiative-convective equilibrium constitutes a classical and convenient paradigm to understand the thermodynamic structure of convective atmospheres, and to investigate its sensitivity to large-scale boundary conditions [*Xu and Emanuel*, 1989; *Emanuel et al.*, 1994]. (In an atmosphere in moist radiative-convective equilibrium, the cooling of the troposphere by radiation is balanced by the warming by convection, and the vertical profile of temperature is close to a moist adiabat.) Here we propose to use the same paradigm to investigate how the vertical distribution of tropical water isotopes depends on large-scale surface and atmospheric boundary conditions.

[34] The simulations are initialized with standard tropical temperature and water vapor profiles, and no heavy water isotopes in the atmosphere. As the ocean constitutes an infinite source of water isotopes, surface fluxes progressively fill the atmosphere with water and heavy isotopes until the input of water and isotopes into the atmosphere is balanced by precipitation. A steady radiative-convective equilibrium is achieved typically in about 20 days.

3. Evaluation Against GNIP Data

[35] The representation of cloud, convective and radiative processes by the SCM has been evaluated against tropical data over the western Pacific warm pool [*Emanuel and Zivkovic-Rothman*, 1999; *Bony and Emanuel*, 2001]. Here we evaluate the model's isotopic simulations in tropical marine locations by using monthly data from the Global Network of Isotopes in Precipitation (GNIP) maintained by the International Atomic Energy Agency (IAEA).

3.1. Tropical Marine Stations

[36] Nine tropical marine stations located over the western Pacific or Indian warm pools or in the tropical Atlantic (Table 4) are selected on the basis of the continuity of the measurements (each station reports at least 4 years of data). Besides, the spatial scale typical of SCM simulations being larger than a few hundreds of kilometers, we select only the stations for which the seasonal cycle of precipitation derived from in situ measurements is consistent with that derived at a larger scale from the Climatic Research Unit (CRU) climatology [*New et al.*, 1999] or the Global Precipitation Climatology Project (GPCP) [*Adler et al.*, 2003]. Then, we force the SCM over a full seasonal cycle by using 6-hourly vertical profiles of large-scale vertical velocity (temperature and moisture forcings are computed consistently) derived from the European Centre for Medium-Range Weather Forecasts Reanalysis (ERA-40) [*Uppala et al.*, 2005], monthly SST data [*Reynolds et al.*, 2002] and a constant background surface wind V_{s0} of 6 m/s (close to the mean surface wind value in the vicinity of these stations).

3.2. Model-Data Comparison

[37] As shown in Figure 2, the model reproduces the main features of the relationships between monthly values of precipitation rate and δD, δ^{18}O and deuterium excess in precipitation (hereafter noted δD_p, $\delta^{18}O_p$ and d_p). Although the model systematically underestimates δD_p by about 18‰ and $\delta^{18}O_p$ by about 2‰ for precipitation rates higher than 2–3 mm d^{-1}, it reproduces well the enhanced depletion of precipitation in heavy isotopes as precipitation increases. This major feature of the tropical isotope behavior is referred to as the "amount effect" [*Dansgaard*, 1964; *Rozanski et al.*, 1993]. To compare more easily the observed and simulated slopes of the precipitation-δD_p relationship, a uniform offset of 18‰ is added to the simulated δD_p (Figure 2c). The simulated amount effect (−4.4‰ mm^{-1} d for δD_p and −0.6‰ mm^{-1} d for $\delta^{18}O_p$) is very close to that derived from observations in the nine tropical marine stations (−4.1‰ mm^{-1} d for δD_p and −0.55‰ mm^{-1} d for $\delta^{18}O_p$). Model and data also show similar dispersion (correlation coefficients between δD and precipitation for the SCM and for observations are −0.80 and −0.87, respectively). For light rains (less than 3 mm d^{-1}), however, the slope of the amount effect derived from the model is about twice that derived from observations (−12‰ mm^{-1} d versus −6.3‰ mm^{-1} d).

[38] The deuterium excess d_p is reasonably well simulated by the model (Figure 2d), including the increase of d with precipitation (0.4‰ mm^{-1} d for observations versus 0.5‰ mm^{-1} d for the model). We note however that the model slightly underestimates the dispersion around the mean relationship (the correlation between d_p and precipitation is 0.39 for observations and 0.55 for the model).

[39] The simulations of the isotopic composition of precipitation thus present two main biases: a systematic underestimate of δD_p in regimes of high precipitation (i.e., for precipitation larger than 2–3 mm d^{-1}), and an overestimate of the δD_p sensitivity to precipitation in regimes of weak precipitation (less than 2–3 mm d^{-1}).

[40] As explained in section 2.4, the first bias may result in part from the one-dimensional framework and the absence of horizontal advections of water isotopes in the model forcing. The second bias is presumably rather related to our representation of isotopic processes in unsaturated downdrafts. In regimes of light rain, drop evaporation is intense and some drops (the smallest ones in particular) may reevaporate totally without fractionation. Taking this effect into account would decrease δD_p all the most that the rain is light,

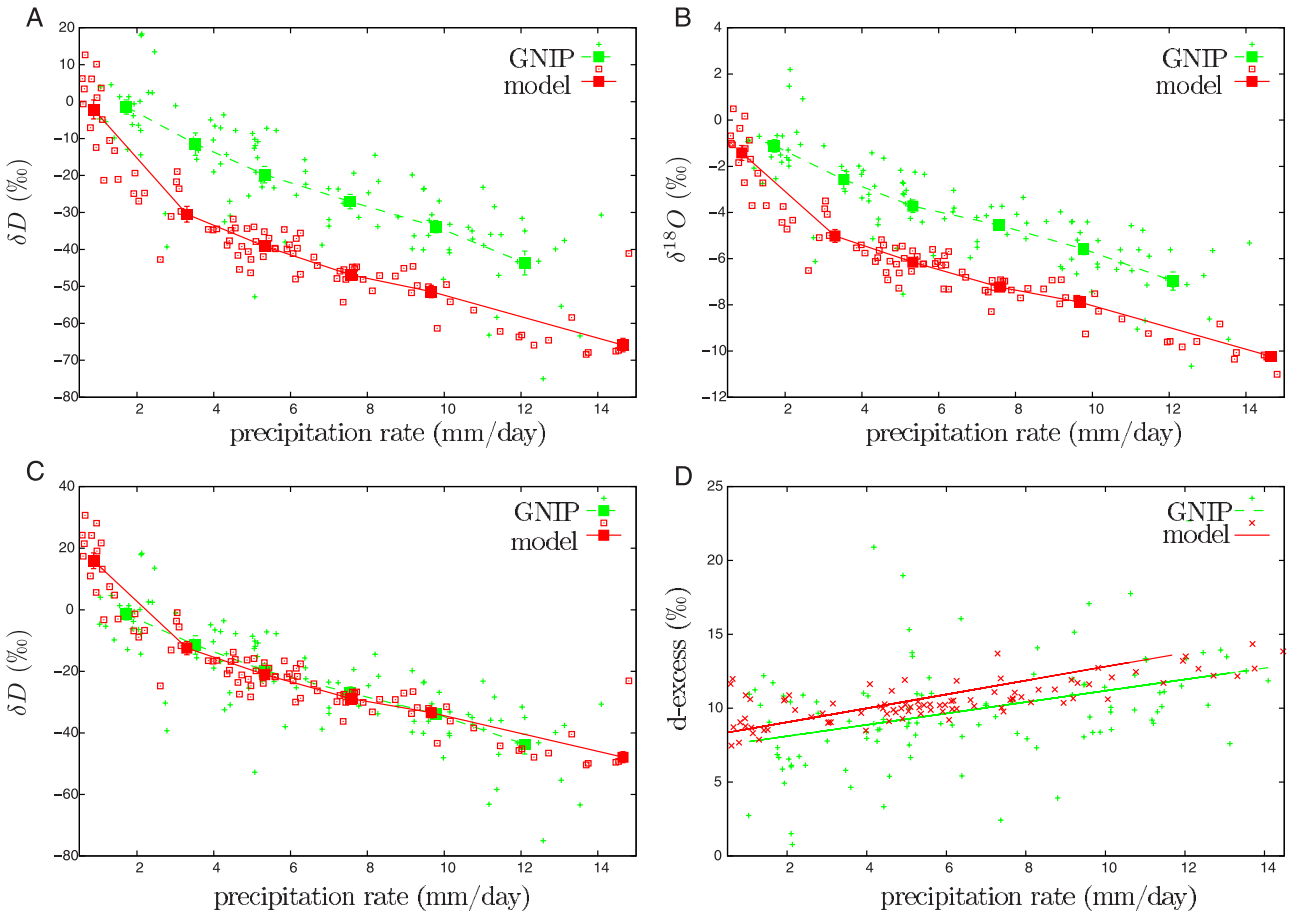

Figure 2. (a) Relationship between monthly values of δD in precipitation and the precipitation rate simulated by the single-column model (solid red line) or derived from the GNIP database (dashed green line) for nine tropical marine stations maintained by the IAEA. Small markers show individual monthly results from observations or simulations. Also reported is the mean relationship between δD and precipitation binned into six bins of precipitation rate values. (b) Same as Figure 2a, but for δ^{18}O. (c) Same as Figure 2a, but after having added an offset of 18‰ to the simulated δD to make the comparison between simulations and observations easier. (d) Relationship between the monthly Deuterium excess (d) in precipitation and the precipitation rate. Also reported are linear regression lines associated with simulations (thick red) and observations (thin green).

and thus would reduce the slope of the δD_p-precipitation relationship in regimes of weak precipitation. This calls for representing explicitly, in the future, the size spectrum of the falling droplets in the model. The assumption that the unsaturated downdraft covers a constant area might also explain part of the bias.

4. Radiative-Convective Equilibrium

[41] Radiative-convection equilibrium simulations are performed (1) to study the sensitivity of the isotopic composition of the precipitation to large-scale boundary conditions and to unravel the dynamical and nondynamical contributions to the amount effect, (2) to examine the sensitivity of the isotopic composition of the precipitation to model parameters, and (3) to investigate the typical vertical distribution of water isotopes in the tropical atmosphere.

4.1. Sensitivity of the Isotopic Composition of the Precipitation to Large-Scale Boundary Conditions

[42] Interpreting quantitatively observed variations of the isotopic composition of precipitation in terms of variables such as surface temperature, precipitation or large-scale circulation would allow us to use stable water isotopes as indicators of climate variations and to reconstruct past climate variations [e.g., *Rozanski et al.*, 1993].

[43] In the tropics, a difficulty hampering such an interpretation is that surface temperatures and the large-scale atmospheric circulation often vary in concert at monthly or longer timescales. On average, the rising branches of the tropical overturning circulation predominantly occur over the areas of warmest surface temperature [*Bony et al.*, 2004], and thus mean precipitation amounts correlate positively with surface temperatures. This correlation results from the ability of the cumulus mass flux (and thus of the upward motion) to adjust to surface temperatures by modulating the subcloud-layer equivalent potential temperature

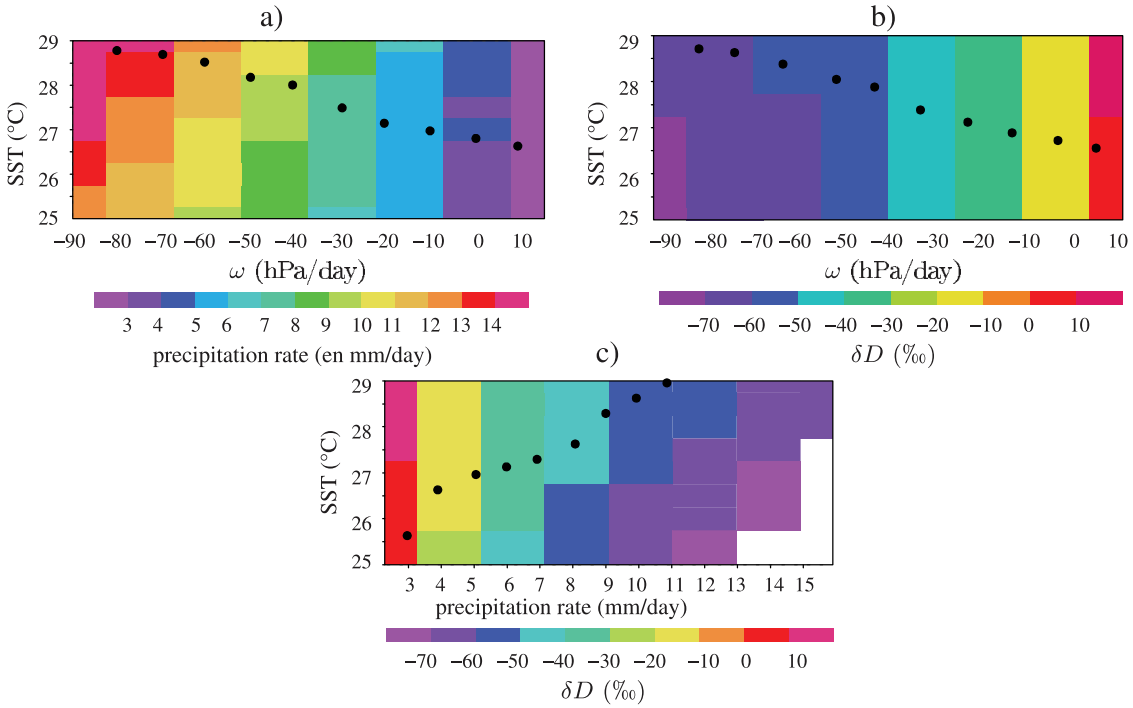

Figure 3. (a) Precipitation (in mm d^{-1}) simulated for different conditions of SST and large-scale forcing (ω). The black dots show the mean statistical relationship between SST and ω derived from reanalysis data [*Bony et al.*, 2004]. (b) Same as 3a but for δD in precipitation. (c)The δD in precipitation (in %) presented as a function of SST and precipitation. The black dots show the mean statistical relationship between SST and precipitation rate derived from the black dots of Figure 3a.

so as to tie, through a moist adiabat, the horizontally variable surface temperatures to the more horizontally uniform temperatures of the free troposphere [*Emanuel et al.*, 1994; *Sobel and Bretherton*, 2000].

[44] Owing to the correlation between surface temperature and large-scale upward motion, the observed decrease of δD_p with increasing surface temperature that is found on average over the tropics [*Rozanski et al.*, 1993] does not necessarily reveal an intrinsic sensitivity of δD_p to temperature.

[45] The SCM reproducing reasonably well the relationship between δD_p (or $\delta^{18}O$) and precipitation in tropical regions (section 3), we use it to investigate how the atmosphere responds either to a change in SST or to a change in large-scale motion, and to quantify the relative influence of both changes on δD_p, $\delta^{18}O_p$ and d_p.

[46] For this purpose, we perform a series of radiative-convective equilibrium simulations using different specified SSTs, and by imposing different profiles of large-scale vertical velocity (section 2.4). As in the tropics nearly all of the upward motion occurs within cumulus clouds and gentle subsidence occurs in between clouds, imposing a large-scale (or ensemble-average) rising motion enhances the cumulus mass flux and thus the convective activity and the precipitation.

4.1.1. Amount Effect

[47] The SST and the maximum large-scale vertical velocity imposed in the midtroposphere vary from 25°C to 30°C and from −90 hPa d^{-1} to +10 hPa d^{-1}, respectively, which are typical ranges of variation in the tropics (regimes of strong large-scale ascent are associated with deep convection while regimes of midtropospheric subsidence are associated with shallow convection). Increases of SST or of large-scale ascent both increase the water input into the atmospheric column and thus the equilibrium precipitation (Figure 3a). However, in the first case, it is through an increase of the surface evaporation while in the second case it is mainly through an enhanced large-scale convergence of atmospheric moisture. For typical tropical conditions, the range of variation of the precipitation is much larger for dynamically induced changes than for SST-induced changes (Figure 3a).

[48] Figure 3b shows that the range of variation of the equilibrium δD_p with SST is much smaller than that with large-scale motion, consistently with the smaller change in precipitation (Figures 3a and 3c). Over tropical oceans, the main control of δD_p is thus the atmospheric circulation.

[49] To investigate the relationship between δD_p and precipitation for realistic correlative variations between SST and ω, we use two different approaches. The first one consists in prescribing the covariation of ω with SST after the mean statistical relationship derived from satellite data and meteorological reanalysis data [*Bony et al.*, 2004]. The second one consists in using the weak temperature gradient (WTG) approximation to diagnose, with the SCM, the vertical velocity ω that would be associated with different SSTs for a given externally prescribed vertical temperature profile in the free troposphere [*Sobel and Bretherton*, 2000]. Details of WTG calculations are given in the Appendix B.

[50] Figure 4 compares the relationship between δD_p and precipitation that is derived from the model when the SST and the large-scale vertical motion vary correlatively (the two approaches yield to comparable results), and when

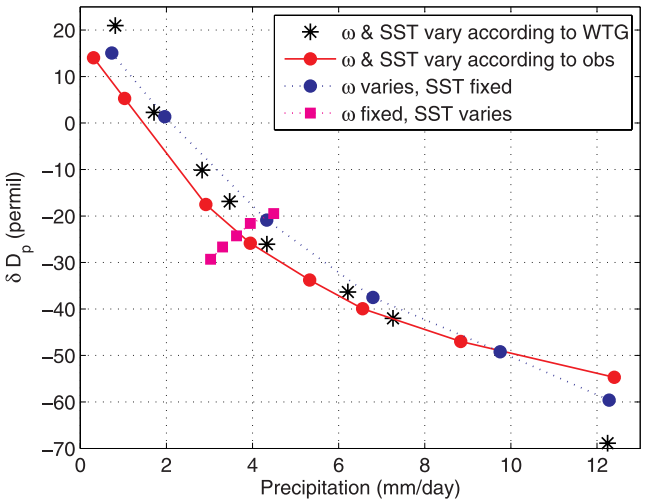

Figure 4. Relationship between δD_p and precipitation derived from radiative-convective equilibrium simulations: when the SST and the large-scale vertical velocity vary correlatively, using either the weak temperature gradient approximation (WTG) (black stars) or a mean statistical relationship derived from satellite data and meteorological reanalyses (red solid line and circles); when the large-scale vertical velocity varies (from −60 to +30 hPa d^{-1}) but the SST is set to 29°C (dotted blue line and circles); when the SST varies (from 20°C to 30°C) and the large-scale vertical velocity is set to 0 hPa d^{-1} (magenta squares).

either the SST or the large-scale motion is kept fixed. The amount effect simulated by the model with varying ω and fixed SST is very close to that simulated when both SST and ω vary: the mean slope is −6.3‰ mm^{-1} d in the first case and −5.3‰ mm^{-1} d in the second case. The amount effect is therefore largely explained by dynamical variations; assuming that it results only from dynamical variations leads to an error of less than 15% in the slope of the relationship between δD_p and precipitation.

[51] Figures 3 and 4 show that for a given large-scale motion, δD_p slightly increases with precipitation as SST increases. The temperature dependence of the fractionation coefficients during condensation has very little impact on this relationship (not shown). Actually, the increase of δD_p with SST despite the concomitant increase in precipitation (an ''anti−amount effect''), is explained by two main reasons. First, when the SST increases the evaporation flux from the ocean (and thus the precipitation) is more enriched. Secondly, owing to the moist adiabatic structure of the tropical troposphere, an increase in surface temperature is associated with a whole tropospheric warming and a decrease of the temperature lapse rate, so that temperatures increase more at altitude than at the surface; this decreases the difference between surface temperature and the average condensation temperature (even for an unchanged average condensation height) and thus the fraction of condensed water ($f_c = 1 - f_v$) in the convective parcels, leading to a reduced depletion of the atmosphere.

[52] These results suggest therefore that the amount effect can be observed only if precipitation variations are associated with large-scale circulation changes. The implications of this finding for the interpretation of long-term isotopic records of δD in precipitation are discussed in section 6. The physical processes underlying the amount effect are extensively discussed in a companion paper [*Risi et al.*, 2008].

4.1.2. Deuterium Excess

[53] The same analysis was conducted for the deuterium excess in precipitation (not shown). The d_p also exhibits little sensitivity to SST (a very slight decrease with SST) but increases with precipitation by about 0.7 mm^{-1} d. In our model, this increase is explained by two main processes. First, the reevaporation of the falling precipitation is weaker in regimes of strong precipitation than in regimes of weak precipitation. Since rainfall reevaporation lowers d in the precipitation, d is higher in regimes of high precipitation. Secondly, when convective updrafts get stronger, unsaturated downdrafts also get stronger and the atmospheric recycling of the subcloud layer vapor by the air advected downward by these downdrafts gets higher. Since the vapor at altitude is associated with a higher d than the subcloud layer (it will be shown later in this paper), this recycling increases the deuterium excess of the subcloud layer feeding the convective system, and thus the whole convective system and the precipitation.

4.2. Sensitivity to Convective and Isotopic Processes

[54] We now examine the sensitivity of the simulated isotopic composition of the precipitation to key model parameters. For this purpose, we perform systematic tests of the radiative-convective equilibrium by perturbing individually the parameters by ±20%. These parameters are mainly related to the representation of cloud physics and microphysics in the convection scheme (they were originally calibrated against TOGA COARE data [*Emanuel and Zivkovic-Rothman, 1999; Bony and Emanuel,* 2001]), in particular to the representation of unsaturated downdrafts and to the calculation of the precipitation efficiency ϵ_p (Table 1). Two other parameters, λ and ϕ, are involved in the representation (and the tuning) of kinetic effects associated with fractionation processes during ice condensation and rain reevaporation, respectively (section 2.3).

[55] The isotopic composition of the simulated precipitation exhibits a significant sensitivity (i.e., when model parameters are perturbed by ±20%, the change in δD_p is larger than the typical accuracy of δD measurements in precipitation which is about 0.5‰) to parameters related to unsaturated downdrafts (Figure 5). In particular, the strong sensitivity to the isotopic parameter ϕ (a variation of ϕ of 40% leads to δD variations of the order of 10‰, of opposite sign in regimes of strong and weak convection) shows that kinetic effects in unsaturated downdrafts crucially control the isotopic composition of tropical precipitation. This is especially true in regimes of weak precipitation which are associated with strong reevaporation of falling rain. Conversely, this points to the potential utility of the isotopic composition of precipitation to better understand the processes associated with the reevaporation of precipitation and to better constrain their representation in large-scale models.

[56] On the other hand, the isotopic composition of the precipitation does not critically depend on the precipitation efficiency. This is because most of the simulated precipitation (more than 90%) originates from the water condensed within the adiabatic updraft, whose isotopic composition does not

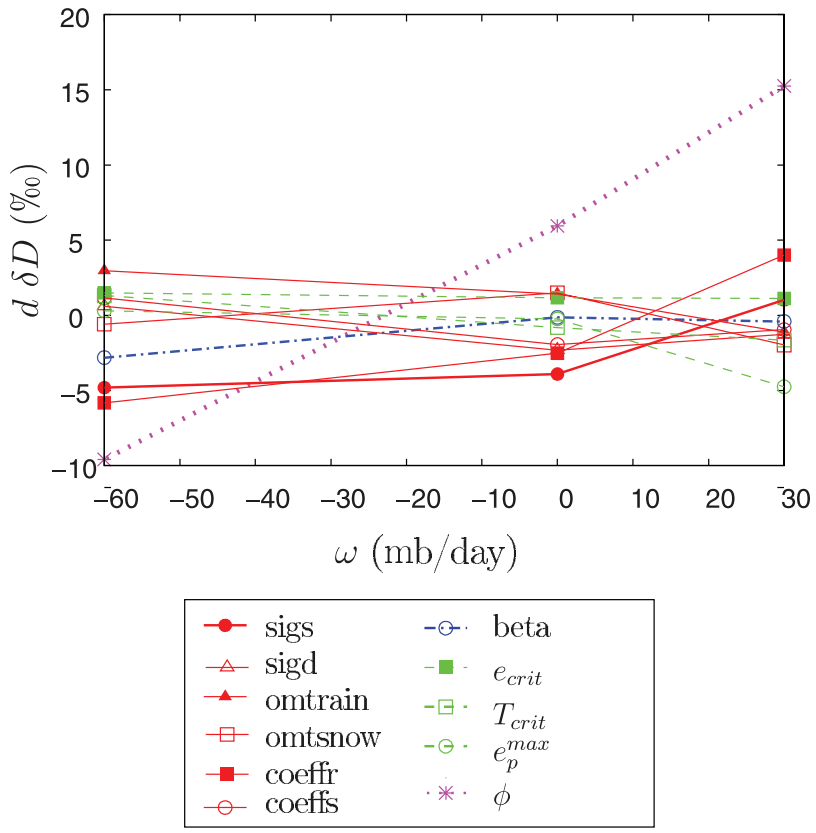

Figure 5. Change in the δD of precipitation simulated when model parameters (defined in Table 1) are individually perturbed by ±20% around their control value. Results are presented for different radiative-convective equilibrium experiments forced by an SST of 29°C and by different magnitudes of large-scale vertical velocity (the values in hPa d^{-1} reported in abscissa refer to the extremum value of the vertical velocity in the midtroposphere). The equilibrium precipitation rates associated with ω values of −60, 0, and +30 hPa d^{-1} are about 12, 4, and 0.7 mm d^{-1}, respectively.

depend on the precipitation efficiency (section 4.3.2). Nevertheless, in the case where ϵ_p varies with height (as in the Emanuel scheme), a change in the vertical profile of ϵ_p might change the composition of the surface precipitation by affecting the vertical origin of the precipitated water. However, the isotopic composition of the condensed water is bounded on the upper side by the composition of the condensate in equilibrium with the subcloud layer vapor, and on the lower side by the isotopic composition of the subcloud layer water vapor (section 4.3.2). It is thus strongly constrained and cannot vary much whatever happens above the subcloud layer.

[57] Consistently, the slope of the simulated amount effect depends sensitively on the parameters related to the representation of convective unsaturated downdrafts, but not on the other ones.

4.3. Vertical Distribution of Water Isotopes

[58] We now examine the typical vertical distribution of water stable isotopes in the tropical atmosphere in the absence of large-scale flow. For this purpose we force the model by a sea surface temperature of 29°C and a background wind speed of 5 m s^{-1}, and run it for about 100 days to approach a radiative convective equilibrium. In the troposphere, such a simulation might be considered as representative of the whole Tropics. However, it is not the case in the uppermost troposphere because in the TTL (above about 14 km or 125 hPa), we do not represent the mean large-scale ascent associated with the Brewer-Dobson circulation. We will thus focus on the distribution of water stable isotopes simulated by the model from the surface up to about 125 hPa.

[59] The variability of the vertical profiles of δD with varying surface conditions and large-scale dynamical forcings will be investigated in section 5.

4.3.1. Main Features

[60] Figure 6a shows the vertical profile of δD simulated at equilibrium in the environment (i.e., outside convective clouds), hereafter noted δD_{env} (the vertical profile of $\delta^{18}O$ being qualitatively similar, we do not show it to avoid repetition).

[61] The δD_{env} decreases with altitude until 175 hPa (about 12.5 km), where is reaches a minimum value (about −460‰). This depletion results from the progressive removal of heavy water isotopes through condensation and precipitation in convective updrafts. At altitudes higher than the 700 hPa pressure level, δD_{env} values are less depleted than would be expected for an air parcel experiencing a Rayleigh distillation. Such a feature is consistent with in situ [*Webster and Heymsfield*, 2003; *Hanisco et al.*, 2007] and

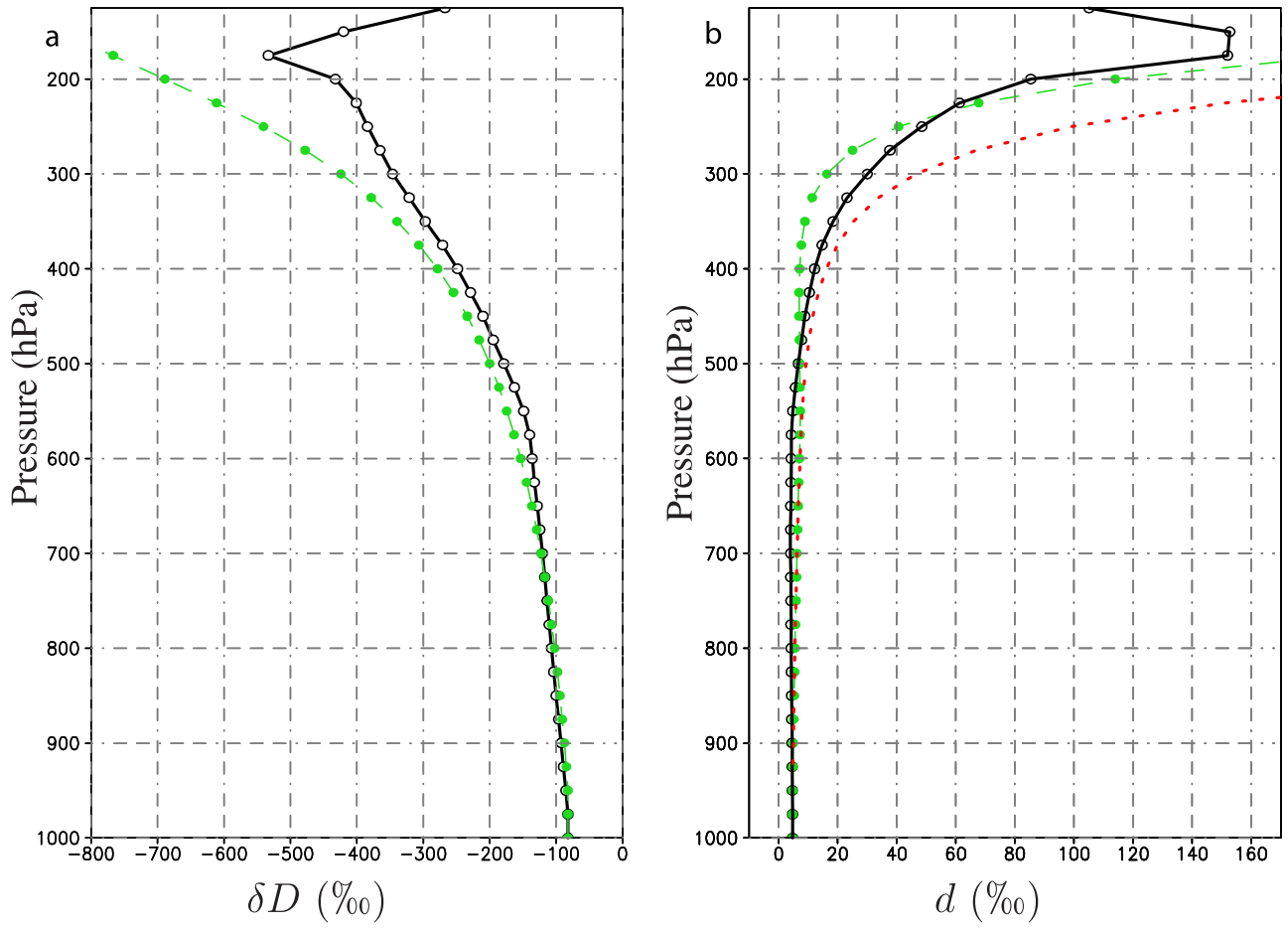

Figure 6. (a) Steady state profiles of δD simulated in the environment in the absence of large-scale flow (solid black line). The profile predicted by the Rayleigh distillation is reported (green dashed line). (b) Equilibrium profiles of d in the environment for the same conditions (solid black line). Also reported is the profile predicted by a Rayleigh distillation by switching on (green dashed line) or off (dotted red line) the kinetic effects associated with ice condensation.

remote [*Kuang et al.*, 2003] isotopic measurements in the tropics. Between 175 hPa and the tropopause (that occurs around 100 hPa in these simulations), δD_{env} progressively increases with altitude. This is in qualitative agreement with the measurements made during the Costa Rica Aura Validation Experiment (CR-AVE) [*Hanisco et al.*, 2007]. The profiles derived from this experiment (http://espoarchive.nasa.gov/archive/arcs/cr_ave/data/wb57/) show quite systematically an enrichment with altitude of the order of 100‰ above 175 hPa.

[62] The deuterium excess in the environment (noted d_{env}) increases drastically with altitude, especially above 400 mb (Figure 6b). Although the accuracy of isotopic measurements in altitude does not allow for an accurate d calculation, CR-AVE data also feature an increase in d with altitude (not shown). Such an increase is also predicted by a Rayleigh distillation, even in the absence of kinetic effects during ice condensation (i.e., by setting the ice fractionation coefficient to its equilibrium value). This points to the fact that the deuterium excess in the troposphere is only partly related to the kinetic effects associated with ice condensation. In the case of a Rayleigh distillation, the increase simply results from the fact that as δ values decrease and tend toward −1000‰ in altitude, d_{env} increases and tends toward 7000‰. In the case of a convective atmosphere, on the other hand, d reaches a maximum value around 175 hPa.

4.3.2. Interpretation

[63] In the tropical free troposphere, the main source of water molecules ($H_2^{16}O$ or heavier isotopologues) is the detrainment of (total) water from cumulus clouds. In our model, water is detrained partly from undiluted (or adiabatic) updrafts, and partly from diluted updrafts and downdrafts (i.e., mixtures of undiluted and environmental air). Figure 7 shows that the isotopic composition of the environment closely follows that (noted δD_{adiab}) of the total water lifted adiabatically from the subcloud layer and detrained into the environment after (partial) precipitation. This is because the total water detrained from diluted updrafts has a composition slightly more depleted but not substantially different from that of undiluted updrafts (not shown).

[64] The vertical profile of δD_{adiab} can be understood by examining the isotopic composition of water in its vapor and condensed phases (Figure 7). As the adiabatic updraft is assumed to loft water faster than the rate at which precip-

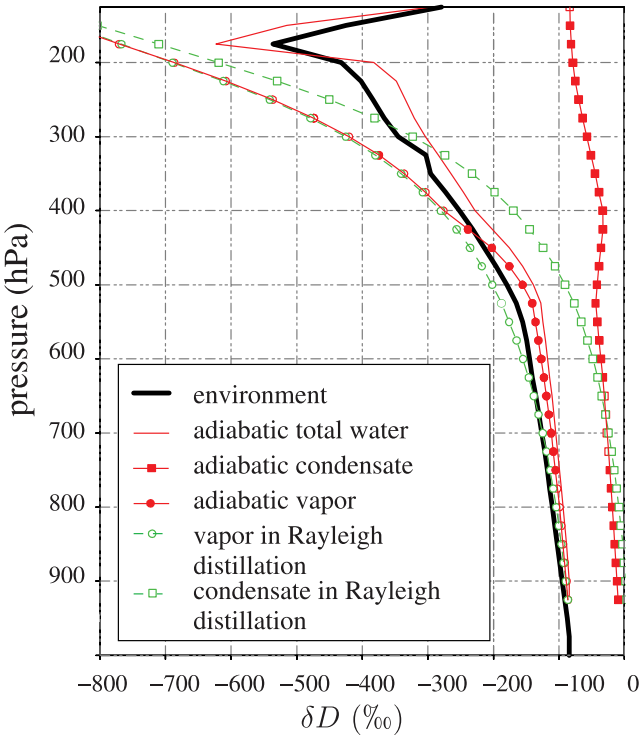

Figure 7. The δD profiles of water vapor in the environment (thick black line), of the total water detrained from the adiabatic updraft after precipitation (δD_{adiab}, thin red line), and of its condensed (red solid squares) and vapor (red solid circles) phases. Also reported are the isotopic compositions of the condensed water (green open squares) and of the water vapor (green open circles) predicted by a Rayleigh distillation.

itation processes start operating, its condensed water is much richer in heavy isotopes than if it were originating from a water parcel already depleted by precipitation (as in a Rayleigh distillation). In the upper troposphere, as nearly all of the water carried upward by the adiabatic updraft is condensed, the composition of the condensed water tends toward that of water vapor in the subcloud-layer, while the remaining water vapor gets very depleted. The composition of the total water is a combination of the compositions in the condensed and vapor phases. The δD_{adiab} thus decreases with altitude in the lower and middle troposphere owing to the strong depletion of the adiabatic vapor with altitude, and increases below the tropopause as the fraction of condensed water within the lofted parcel tends to unity.

[65] This can be explained analytically by considering the evolution with height of the isotopic composition of an air parcel lofted by an adiabatic updraft and for which a fraction ϵ_p of the condensed water is converted into precipitation at each vertical level (in the Emanuel's scheme, this fraction is calculated according to equation (1) and thus varies with height, but here we set it to a constant value for the sake of simplicity). We will apply this model to humidity and temperature profiles typical of a tropical atmosphere in radiative-convective equilibrium. Let q_t and X_t be the mixing ratios of "normal" and "heavy" total water, and $R_t = X_t/q_t$ the corresponding isotopic ratio. In the absence of precipitation, R_t would be conserved during the ascent and equal to the isotopic ratio of the subcloud-layer water vapor R_o. In the presence of precipitation, the mixing ratios of the air parcel become $q'_t = q_v + (1 - \varepsilon_p)q_c$ and $X'_t = X_v + (1 - \varepsilon_p)X_c$ (the subscripts v and c refer to water in its vapor and condensed phases), and the isotopic ratio is given by $R'_t = R_t\left(\frac{1-\epsilon_p\frac{X_c}{X_t}}{1-\epsilon_p f_c}\right)$, where f_c is the fraction of condensed water in the parcel before precipitation ($f_c = q_c/q_t = 1 - f_v$). In the absence of equilibration between vapor and condensate (which is the case when the condensate is frozen), $R_v = R_o(1 - f_c)^{\alpha-1}$, where α is the fractionation coefficient, and thus $X_c/X_t = 1 - (1 - f_c)^{\alpha}$. It follows that

$$\frac{R'_t}{R_o} = \frac{1 - \epsilon_p + \epsilon_p(1 - f_c)^{\alpha}}{1 - \epsilon_p f_c}. \tag{2}$$

[66] In the absence of precipitation ($\epsilon_p = 0$), $R'_t = R_t = R_o$. If $\epsilon_p = 1$, all the condensate is precipitated out: this situation corresponds to a Rayleigh distillation and is not accompanied by any enrichment in the upper troposphere. In the general case where $0 < \epsilon_p < 1$, part of the condensate lofted by convection remains within the parcel. The evolution of the isotopic ratio of the parcel as it rises is illustrated by Figure 8 for different values of ϵ_p. As expected, the isotopic ratio of the vapor and of the condensate depend only on f_c and α and do not depend on the precipitation efficiency ϵ_p (Figure 8a). As the parcel rises, f_c increases (Figure 8b) and δD decreases (Figure 8c). In the uppermost troposphere, f_c tends to unity and thus fractionation and precipitation processes do not affect R_t anymore: δD tends to R_o whatever $\epsilon_p < 1$ (Figure 8c). A parcel rising adiabatically to temperatures cold enough to condense nearly all of its water content has thus an isotopic ratio similar to that of the near-surface air. As ϵ_p increases, the value of the minimum δD decreases (the air is more depleted), and the altitude at which this minimum occurs increases. Sensitivity tests show that the isotopic kinetic effects associated with frozen condensation have a negligible impact on the vertical profile of δD.

[67] These results thus show that the increase with altitude of δD in the upper troposphere is specific to convective situations in which updrafts are strong enough to loft condensed water. This confirms that the isotopic composition of water in the upper troposphere is a good tracer of convective transports of atmospheric water [*Webster and Heymsfield*, 2003; *Hanisco et al.*, 2007]. As emphasized by *Schmidt et al.* [2005], this also suggests that a careful comparison of observed and simulated profiles of δD in the upper troposphere (even well below the tropopause) would help to constrain some poorly known parameters of convection schemes. Currently, the maximum value of ϵ_p in the Emanuel's convection scheme is set to 0.999 to predict cloud water contents that optimize the comparison of observed and predicted relative humidity and top-of-atmosphere radiative fluxes [*Bony and Emanuel*, 2001]. In the future, this value might be updated so as to optimize the simulation of both relative humidity, radiative fluxes and upper tropospheric δD.

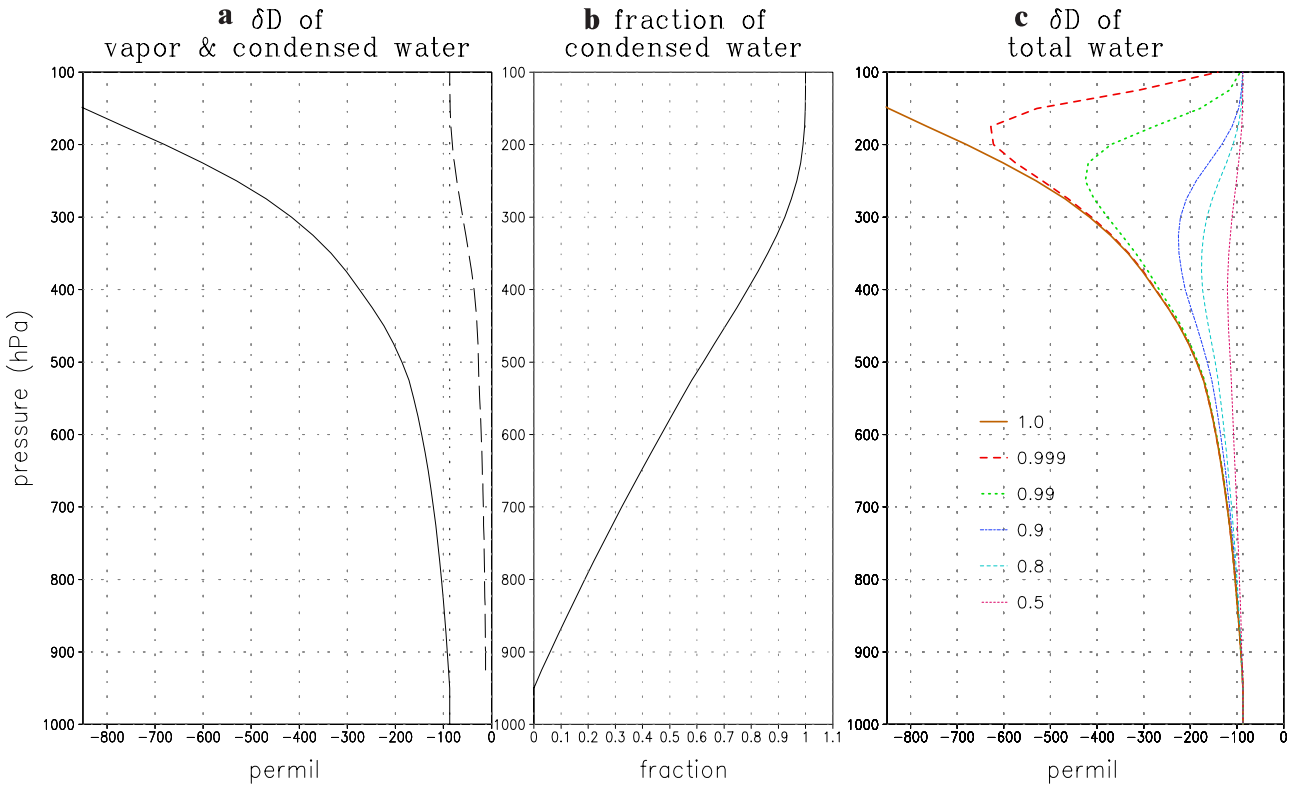

Figure 8. (a) Vertical profiles of isotopic ratios (expressed as δD, in ‰) of vapor (solid line) and condensed water (dashed line) within an air parcel rising in an adiabatic updraft. (b) Fraction of condensed water (f_c) within the updraft. (c) Isotopic ratio of total water detrained from the adiabatic updraft after precipitation. Results are shown for different values of the precipitation efficiency ϵ_p. When the results do not depend on ϵ_p, only one line (in black) is shown.

4.3.3. Sensitivity to Model Parameters

[68] As expected from the previous discussion and consistently with Figure 8, the vertical profile of δD above 400 hPa is very sensitive to the two parameters involved in the calculation of ϵ_p (T_{crit} and $\epsilon_p^{\max}$, see equation (1)), especially above 175 hPa (not shown). In particular, when $\epsilon_p^{\max}$ is set to unity, no condensate is detrained from the cloud into the environment, and the model does not simulate any isotopic enrichment in the upper troposphere anymore. The sensitivity of δD to other model parameters is weaker and smaller than the typical accuracy of isotopic measurements in the upper troposphere (about 50‰) [*Hanisco et al.*, 2007]. This is the case in particular with the sensitivity of δD to isotopic kinetic effects associated with the formation of ice in the presence of sursaturation (not shown).

5. TOGA-COARE

[69] The TOGA-COARE campaign was conducted from November 1992 to February 1993 over the western Pacific warm pool, over a region of roughly 500 km across centered around 2°S and 155°E. This region of high SST (29.4°C on average during the 4 months) is characterized by a strong convective activity and a pronounced intraseasonal variability [*Chen et al.*, 1996].

[70] Although there were no isotopic measurements during this campaign, our main motivations for simulating the isotopic composition of the atmosphere during TOGA-COARE are threefold. First, the Emanuel's convective parameterization has been optimized using TOGA COARE data [*Emanuel and Zivkovic-Rothman*, 1999]. Second, the large atmospheric variability observed during the campaign makes it possible to examine how the isotopic composition of the atmosphere evolves together with the convective activity under a time-varying large-scale forcing and using a less idealized framework than the radiative-convective equilibrium. In particular, it makes it possible to examine the robustness of the δD-convection relationship at timescales shorter than that typically associated with radiative-convective equilibrium. Finally, several studies have used water isotopes to investigate the mechanisms through which air is transported from the upper troposphere to the lower stratosphere [*Rosenlof*, 2003; *Dessler et al.*, 2007]. Examining the isotopic composition of the air detrained from cumulus clouds over the western tropical Pacific area during the November–February period is of particular interest for this purpose because it is where and when most of the troposphere-stratosphere exchanges are likely to occur [*Newell and Gould-Stewart*, 1981].

5.1. Atmospheric Simulations

[71] We force the single-column model by TOGA-COARE soundings data derived from the Intensive Flux Array (IFA) during the 120 days of operation of the intensive observing period (IOP). As explained by Emanuel and Zivkovic-Rothman [1999], the data have been corrected

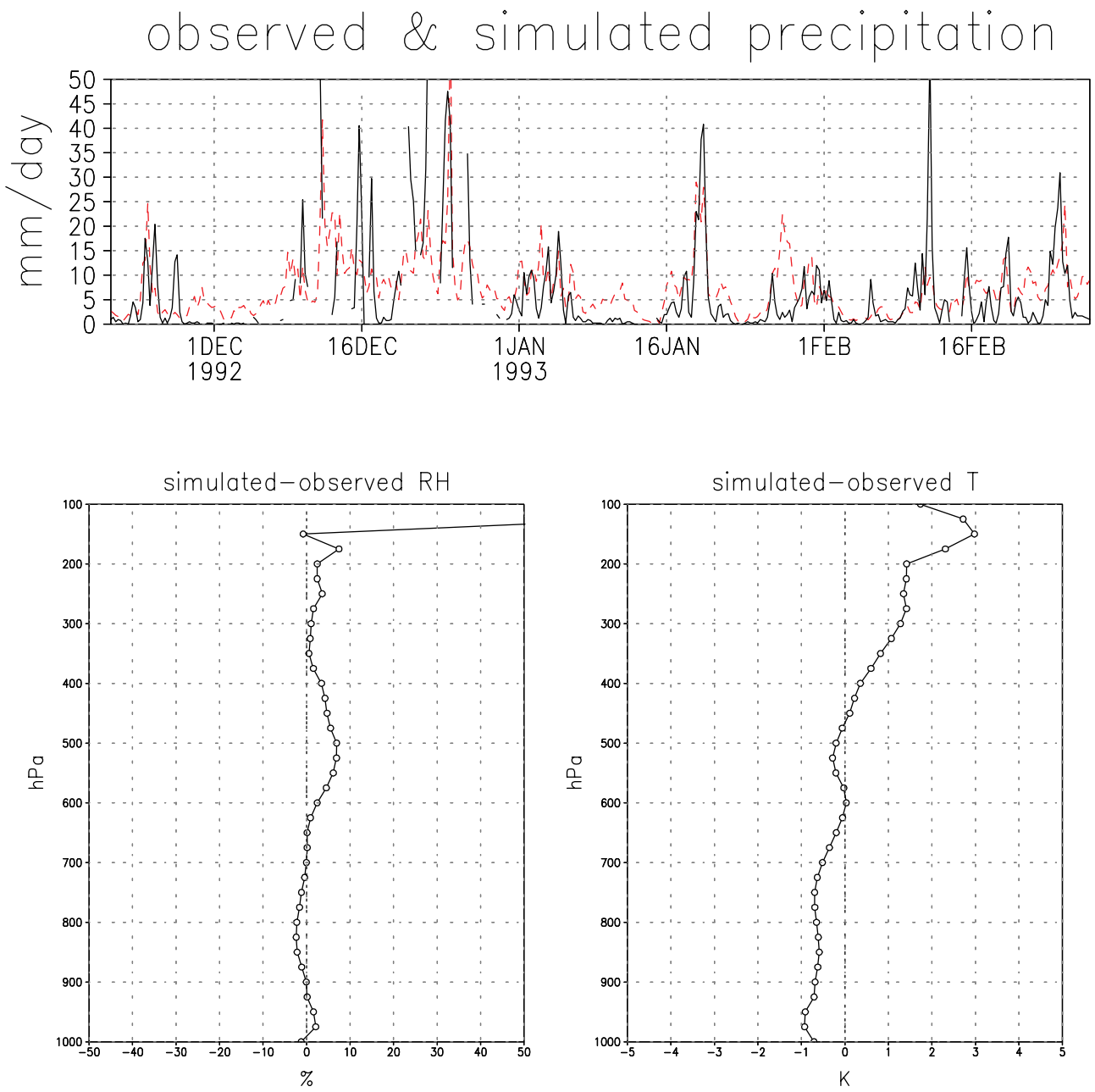

Figure 9. (top) Comparison of the simulated (dashed red line) and observed (solid black line) evolutions of the precipitation over the last 100 days of operation of the TOGA COARE IOP. (bottom) Difference between predicted and observed relative humidity and temperature profiles averaged over the same period.

to ensure the conservation of the column-integrated enthalpy during the experiment. A limitation of the TOGA COARE forcing data set is that large-scale advections of condensate and water isotopes are not available. Therefore we assume in the simulations that there are no large-scale advections of cloud condensate. Vertical advections of water isotopes are thus inferred from the large-scale vertical velocity derived from observations, and large-scale horizontal advections of water isotopes are computed by assuming that they do not modify isotopic ratios. As discussed in sections 2.4 and 3, this assumption is likely to lead to a systematic overdepletion of the convective atmosphere simulated over the IFA. The simulations are initialized by isotopic profiles in a state of radiative-convective equilibrium, and they are analyzed over the last 100 days of operation of the IOP, when the results do not depend anymore on the initial state.

[72] Besides the simulation of water isotopes, the simulations presented here are identical to those presented by *Bony and Emanuel* [2001]. The relative humidity profile simulated by the model is biased by less than 8% on average, and the temperature by less than 1.2 K (Figure 9). Vertically averaged between the surface and 300 hPa (humidity measurements are not reliable above the 300 hPa level), the root-mean-square error of relative humidity is 14% and

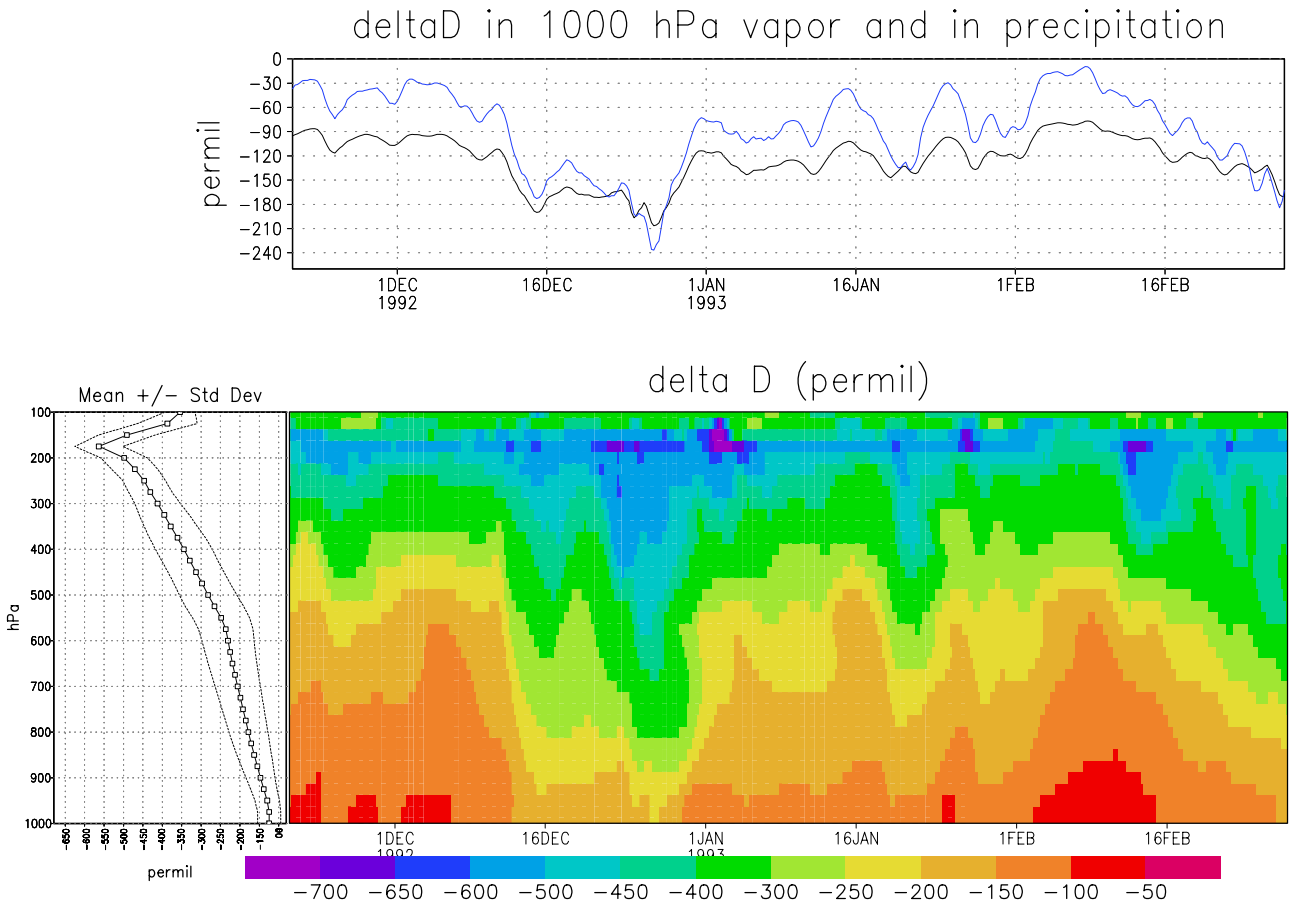

Figure 10. (top) Evolution of δD (in ‰) in the precipitation (blue line) and in the 1000 hPa water vapor (black line) simulated during the last 100 days of operation of the TOGA COARE IOP. (bottom) Evolution of the vertical profile of δD (in ‰) in the environment simulated during the same period. The averaged vertical profile of δD (± the standard deviation) computed over the 100 days is shown on the left.

that of temperature 1.99 K. The model reproduces some of the main characteristics of the cloudiness observed over the warm pool, including the minimum of cloudiness between 600 and 800 hPa, the formation of upper tropospheric anvils associated with mature convective systems and the presence of an extensive layer of thin cirrus clouds just below the tropopause. Radiative fluxes at the top of the atmosphere are in good agreement with satellite observations during periods of active convection, but are in relatively less agreement during periods of suppressed convection owing to a lack of boundary-layer clouds in the simulations.

5.2. Isotopic Compositions

[73] The deep convective activity during the TOGA COARE experiment has been shown to be strongly modulated by tropical intraseasonal oscillations, with the passage in particular of strong and organized super cloud cluster during the last week of December 1992 [*Yanai et al.*, 2000]. Consistently, the isotopic compositions of water vapor and precipitation simulated by the model also exhibit large intraseasonal variations (Figure 10). Higher (i.e., less depleted) δD values are simulated during periods of suppressed convection and low precipitation, and lower (i.e., more depleted) δD values are simulated during sustained periods of deep convective activity and strong precipitation (e.g., during the second half of December 1992). Despite some apparent anticorrelation between low-frequency (i.e., monthly or longer) variations of isotopic ratios and precipitation, the correlation between both variables breaks down at high frequency: δD values at a given time depend not only on the precipitation amount at this time, but also on the convective activity that took place during the previous days or weeks. The timescales associated with the relationship between deep convection and the isotopic composition of water vapor or precipitation are discussed in a companion paper [*Risi et al.*, 2008].

[74] On average over the last 100 days of the IFA, the model simulates δD values of −82‰ ± 50‰ in precipitation and −120‰ ± 30‰ in water vapor at 1000 hPa, and δ^{18}O values of −15‰ ± 8‰ in precipitation and −19‰ ± 5‰ in low-level water vapor. The isotopic ratios in water vapor simulated over most of the TOGA COARE IOP lie in the range of values measured during other tropical field experiments over ocean (*Lawrence et al.* [2004] report δD values ranging from −181‰ to −77‰ and δ^{18}O values ranging from −24‰ to −12‰ at Puerto Escondido (Mexico), and δ^{18}O values ranging from −20‰ to −9‰ during the Kwajalein Experiment KWAJEX). On the other

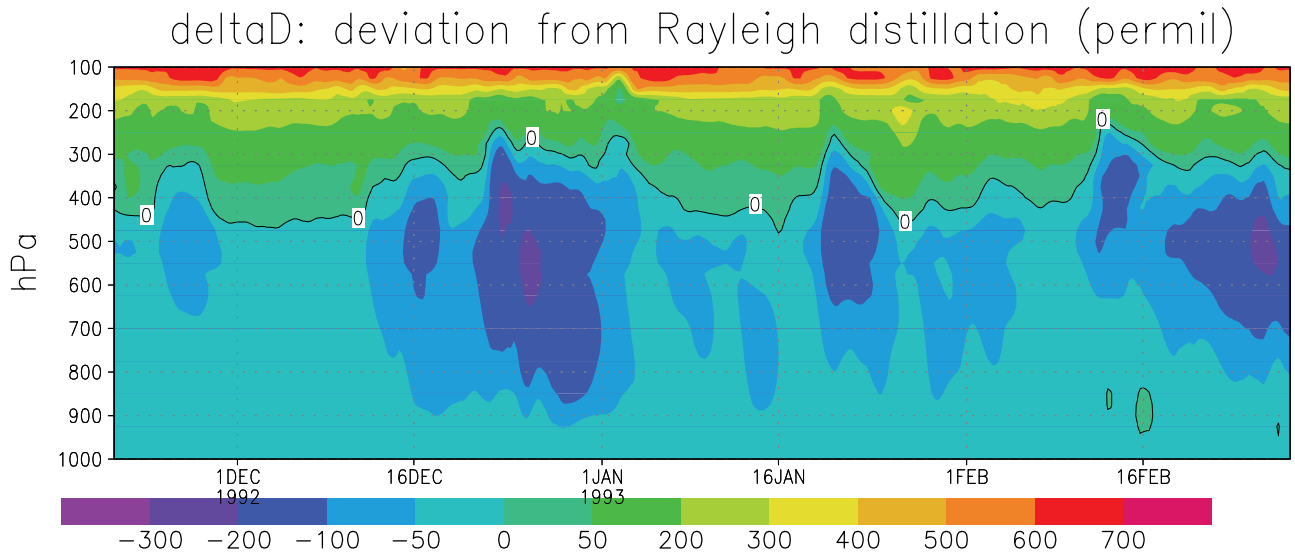

Figure 11. Difference (in ‰) between the vertical profile of δD simulated by the single-column model during the TOGA COARE IOP and that expected from a Rayleigh distillation.

hand, the δ^{18}O values of precipitation in our TOGA COARE simulation are somewhat lower than those measured during KWAJEX (*Lawrence et al.* [2004] report values ranging from −12‰ to −2‰), even for comparable precipitation rates. The reasons for this difference are unclear. This might be due to an excessive reequilibration of the precipitation with water vapor in the model. Alternatively, this might be explained by the fact that the convective systems sampled during KWAJEX were poorly organized [*Lawrence et al.*, 2004] and occurred in environmental conditions different from those prevalent during TOGA COARE.

[75] The simulated vertical profiles of isotopic ratios exhibit several remarkable features.

[76] 1. The temporal evolution of the water vapor isotopic composition shows that δD is much more variable (at least by a factor of 2) in the free atmosphere than near the surface, especially in the middle and upper troposphere. This feature is consistent with aircraft observations [*Webster and Heymsfield*, 2003].

[77] 2. In the lower troposphere δD is generally close to that expected from a parcel of air that would experience a Rayleigh distillation, except during episodes of intense convection (e.g., at the end of December 1992), where it is slightly more depleted (Figure 11). Such a feature has been observed in recent satellite measurements in a large fraction of tropical moist regions [*Worden et al.*, 2007]. In our model, this results mainly from the enhanced compensating subsidence in the environment (the compensating subsidence is the downward mass flux in the environment that compensates the upward mass flux by mass continuity) that advects downward depleted air from high altitudes. The large relative humidity of the lower troposphere during episodes of strong convection, which favors the depletion of water vapor through diffusive exchange processes with the falling precipitation, also contributes to the low δD values of water vapor [*Lawrence and Gedzelman*, 1996]. In the upper troposphere, on the contrary, the isotopic composition of water vapor exhibits a large enrichment compared to a Rayleigh distillation.

[78] 3. As in radiative-convective equilibrium, up to 175 hPa (about 12.5 km) the air gets more and more depleted in heavy isotopes as altitude increases. At higher altitudes, δD exhibits a systematic increase with height. In these simulations, the level of neutral buoyancy occurs around 150 hPa (around 13 km), but deep convective updrafts are allowed to overshoot this level and reach the tropopause level (75–100 hPa or about 15–16 km). The model simulates a maximum of convective detrainment between 150 and 200 hPa (around 12–13 km). Therefore it predicts a minimum of δD approximately at the level of maximum convective detrainment (which occurs slightly below the level of neutral buoyancy and well below the tropopause), and predicts an isotopic enrichment of the atmosphere with height above this level. As explained in section 4.3.2, the shape of the vertical profile of δD, and in particular the height at which δD is minimum, is related to vertical profile of the fraction of condensed water over total water in the lofted parcels. Therefore, the fact that the height of minimum δD corresponds roughly to the height of maximum convective outflow is a coincidence.

[79] The comparison of TOGA-COARE simulations with radiative-convective equilibrium simulations shows that the isotopic enrichment of the upper tropospheric water vapor is found both under steady and transient forcings and thus constitutes a robust signature of deep convective activity. On the other hand, the overdepletion, compared to a Rayleigh distillation, of the lower tropospheric water vapor seems rather specific of transient periods of intense deep convection. Finally, the precipitation δD is much less correlated to the precipitation rate at short timescales than at monthly or longer timescales. This feature is discussed extensively in a companion paper [*Risi et al.*, 2008].

6. Summary and Discussion

[80] Water stable isotopes have been implemented into a single column model whose representation of atmospheric moistening by convection, cloud radiative effects and iso-

topic composition in precipitation has been evaluated against tropical data from the western pacific warm pool. The use of a single column model and of a deliberately simple framework (e.g., radiative-convective equilibrium, ocean conditions) precludes any claim that we are representing all the complexity of the tropical isotope behavior. The aim of this study is rather to better understand how cumulus convection, together with surface and large-scale dynamical conditions, control the isotopic composition of atmospheric water and precipitation in the tropics.

6.1. Precipitation δD

[81] The analysis of the sensitivity to large-scale conditions of δD in the precipitation in a state of radiative-convective equilibrium shows that the amount effect (i.e., the decrease of δD with increasing precipitation on monthly or longer timescales) is observed if precipitation variations result from changes in the large-scale vertical motion of the atmosphere. A detailed analysis of the amount effect, in particular of the physical convective processes underlying it and of the characteristic timescales, is presented in a companion paper [*Risi et al.*, 2008]. An increase in precipitation induced by an increase of surface temperature not associated with a change in large-scale vertical motion leads on the contrary to an ''anti–amount effect'' (i.e., a higher δD_p for a larger precipitation). In this latter case, the increase in precipitation and surface temperature is associated with a decreased difference between the surface temperature and the average condensation temperature (a consequence of the moist adiabatic structure of the tropical atmosphere), and thus with a reduced depletion of the rising parcels.

[82] Large-scale dynamical changes mainly occur in association with modifications of the large-scale horizontal gradients of SST [*Lindzen and Nigam*, 1987]. If the perturbation of tropical SSTs is more uniform in the case of a global climate change than in the case of spatial or short-term (seasonal, interannual) variations, the relationship between surface temperature and δD_p might thus be different in both cases. Therefore, as pointed out for the analysis of tropical cloud feedbacks [e.g., *Hartmann and Michelsen*, 1993; *Bony et al.*, 1997], relationships between δD_p and surface temperature derived from short-term spatiotemporal climate variations might not constitute a useful analogy of the relationship associated with long-term climate changes. However, the analysis and the understanding of the short-term variability of δD_p constitutes the most promising way to better understand the processes that control the behavior of tropical water isotopes, which will ultimately contribute to a better interpretation of long-term changes in δD.

6.2. Vertical Profiles of δD

[83] Radiative-convective equilibrium simulations as well as TOGA-COARE simulations show that the vertical profile of δD in convective atmospheres exhibits several robust characteristics. One of them is that the lower troposphere can be more depleted in heavy isotopes than predicted by a Rayleigh distillation when atmospheric convection is very intense. This feature has been observed in moist regions of the tropics [*Worden et al.*, 2007].

[84] Another characteristic is that the upper tropical troposphere is less depleted in heavy isotopes than a Rayleigh distillation would predict. This feature, which has been well observed [e.g., *Moyer et al.*, 1996; *Webster and Heymsfield*, 2003; *Kuang et al.*, 2003; *Hanisco et al.*, 2007], is mainly due to the fact that strong convective updrafts carry condensed water upward at a faster rate than the time required for precipitation to become efficient (kinetic effects associated with the condensation in supersaturated conditions has a negligible impact in comparison). This has two consequences. First, a parcel of air detrained from cumulus updrafts is much richer in heavy isotopes than a parcel of air that would rise slowly and thus for which condensation would form from a vapor already depleted by precipitation. Second, a parcel rising adiabatically to temperatures cold enough to condense nearly all of its water content has an isotopic ratio that tends toward that of the air at its origin level (generally the near-surface air). In our model, this explains why δD reaches a minimum around 150–200 hPa (12–13 km) and increases at higher altitudes. This may also explain the very high values and the large variability of the isotopic ratios measured in situ (at the small scale) in the vicinity of the tropopause [*Webster and Heymsfield*, 2003; *Gettelman and Webster*, 2005].

[85] The height of maximum convective detrainment occurs around 12–13 km in the tropics (as well as in TOGA COARE simulations) owing to the sharp decrease of the tropospheric radiative cooling rate above this altitude [*Folkins et al.*, 1999; *Hartmann et al.*, 2001]. The air detrained at this height by convection is likely to be subsequently mixed by turbulent processes and transported both horizontally and vertically (outside the warm pool region) up to the lower stratosphere by the large-scale tropospheric circulation, gravity waves and the ascending branch of the Brewer-Dobson circulation [*Johnson et al.*, 2001; *Sherwood and Dessler*, 2001; *Küpper et al.*, 2004]. Our model does not represent these processes and thus cannot simulate the mean isotopic composition of the air within the TTL and at the entry of the lower stratosphere.

[86] However, we note that near the level of neutral buoyancy (which is the height at which most of convective clouds detrain and which corresponds to the bottom of the TTL), our model predicts an isotopic composition of the air ranging from −400‰ to −650‰ (Figure 10). This range of δD values is close to that measured in the lowest stratosphere [*Moyer et al.*, 1996; *Kuang et al.*, 2003; *Hanisco et al.*, 2007; *Nassar et al.*, 2007]. The resemblance between the values measured in the lowest stratosphere and the values predicted by our model at the bottom of the TTL is consistent with the observation that, on average, the vertical profile of δD is nearly uniform within the TTL [*Kuang et al.*, 2003]. It is also consistent with the suggestion by Dessler and Sherwood [2003] that the isotopic composition of the air injected at the bottom of the TTL by deep convection determines, through a combination of convective overshooting, turbulent mixing and large-scale transports, the average isotopic composition of the air throughout the TTL.

6.3. Limitations of the Model and Future Work

[87] The strong sensitivity of the isotopic composition of the precipitation and of the upper tropospheric water to some convective and microphysical parameters (such as those involved in unsaturated downdrafts or in the calcula-

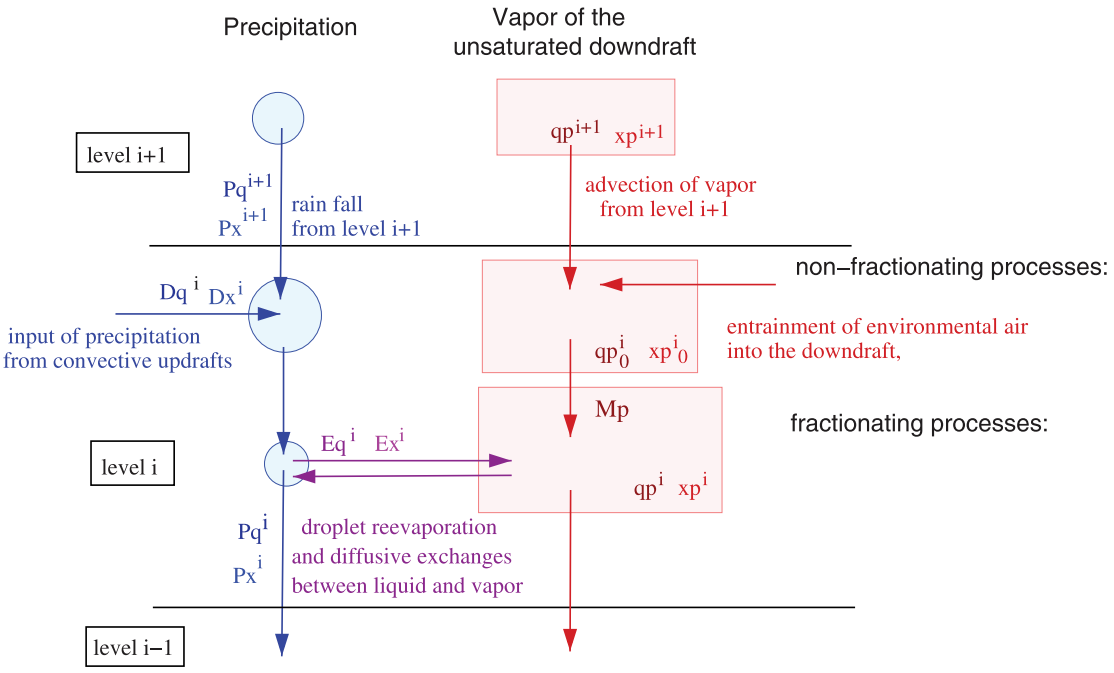

Figure A1. Various fluxes for precipitation and vapor in the unsaturated downdraft.

tion of the precipitation efficiency), highlights the importance of a detailed representation of convective and microphysical processes for an accurate simulation of water isotopes in the tropics. Conversely, as discussed by *Schmidt et al.* [2005], this points to the potential use of isotopes to better understand some convective processes and better constrain their representation in large-scale models.

[88] Several specificities of our model would need to be examined further and evaluated using observations. For instance, the precipitation efficiency ϵ_p (equation (1)), which controls the amount of lofted water detrained into the environment, tends to a constant at low temperatures. Although this constant is poorly constrained from observations (here we use the value from *Bony and Emanuel* [2001] that optimizes the prediction of relative humidity below 300 hPa and of radiative fluxes at the top of the atmosphere), it is critical for the prediction of the water content and the isotopic composition in the upper troposphere (section 4.3.3). Within the TTL (at altitudes above about 125 hPa), *Sherwood and Dessler* [2001] would find it more justified to retain an amount of ice in constant proportion to the saturation mixing ratio of vapor. There is no doubt that the representation of cloud microphysical processes in our model will have to be improved in the future as reliable satellite measurements of upper tropospheric ice amounts and isotopic ratios become available. Including water isotopic measurements (both in the precipitation and in the water vapor from the surface to the upper atmosphere) in future field experiments devoted to the study of convective and cloud processes would also be extremely beneficial. In particular, in the upper troposphere it would help to constrain some microphysical parameters of deep convective clouds such as the precipitation efficiency, while in the lower troposphere it would help to constrain the diffusive exchange processes that take place between the falling raindrops and the surrounding water vapor.

[89] The present study presents many limitations. Some of them are related to the unidimensional and idealized framework of our study. The impact that the horizontal advection of air masses might have on the composition of the convective precipitation cannot be studied simply. Moreover, the response of δD and d excess to changes in surface temperature, large-scale motion and precipitation can be different over ocean and land regions. For this reason, we are currently introducing water stable isotopes in the LMDZ general circulation model, which also uses the Emanuel convection scheme [*Hourdin et al.*, 2006]. Finally, the rigorous evaluation of the model is hampered by the lack of isotopic data in the tropics. For this purpose, we participated in the intensive observing phase of the AMMA (African Monsoon Multidisciplinary Analysis) campaign (http://www.amma-international.org) to collect rainwater samples and to investigate, from the timescale of convective storms to the intraseasonal timescale, the relationship between the isotopic composition of the rain and convective activity. These results will be reported in a future paper.

Appendix A: Isotopic Fractionation in Unsaturated Downdrafts

[90] This appendix explains how isotopic processes in the unsaturated downdraft (reevaporation of precipitation and diffusive exchanges between rain and vapor) are treated in the model. Figure A1 illustrates the unsaturated downdraft processes, their representation and the notations used.

A1. Outline of the Calculation

[91] We divide unsaturated downdrafts processes at level i into two categories: first, processes involving no fractionation (detrainment of condensed water from convective updrafts into the downdraft, entrainment of environmental air, advection of vapor and precipitation from the level above), and second, potentially fractionating processes (reevaporation of precipitation, diffusion between cloud

droplets and the unsaturated vapor). It is assumed here that non fractionating processes occur first, as illustrated in Figure A1.

[92] We call P^i_{q0} and q^i_{p0} the precipitation flux and the vapor mixing ratio respectively after nonfractionating processes occur, and P^i_q and q^i_p the precipitation flux and the vapor mixing ratio respectively after fractionating processes occur. Likewise, we define P^i_{x0}, x^i_{p0}, P^i_x and x^i_p the isotopic counterparts of P^i_{q0}, q^i_{p0}, P^i_q and q^i_p.

[93] We explain here how to calculate P^i_x and x^i_p knowing P^i_{q0}, q^i_{p0}, P^i_q, q^i_p, P^i_{x0} and x^i_{p0}. The calculation is different in the case of snow or rain.

A2. Ice Reevaporation

[94] Since diffusivities in ice are very low, sublimation is assumed not to fractionate, and the isotopic composition of the evaporative flux is then equal to that of the droplet before reevaporation,

$$\frac{E^i_x}{E^i_q} = \frac{P^i_{x0}}{P^i_{q0}}$$

[95] The isotopic composition of precipitation and vapor is then deduced from the isotopic mass conservation equations for the precipitation and the vapor,

$$P^i_x = P^i_{x0} + E^i_x$$
$$x^i_p = x^i_{pO} + \frac{E^i_x}{\tilde{M}_p}$$

where $\tilde{M}_p$ is either M^i_p for an entraining downdraft or M^{i+1}_p for a nonentraining downdraft

A3. Droplet Reevaporation

[96] Let us consider a droplet of isotopic ratio R_l evaporating in the vapor of the unsaturated downdraft of isotopic ratio R_b and relative humidity h_b. According to *Stewart* [1975], the isotopic ratio of the evaporation flux, R_E is

$$R_E = \left(\frac{D'}{D}\right)^n \cdot \frac{\frac{R_l}{\alpha_{eq}} - h_{eff} \cdot R_b}{1 - h_{eff}}, \tag{A1}$$

where α_{eq} is the isotopic equilibrium fractionation factor over liquid, and D the diffusivity of H^{16}_2O, D' the diffusivity of the isotope considered, n an exponent that depends on drop size (set to 0.58 is the model, which corresponds to drop about 1 mm in diameter) and $h_{eff} = h_b$.

[97] Because the vapor around the droplet gets humidified by the evaporating droplet, we assume that h_{eff} is actually intermediate between h_b and relative humidity at saturation ($h_s = 1$). For simplicity, we just assume h_{eff} remains constant throughout the evaporation processes and approximate it by: $h_{eff} = \phi \cdot h_s + (1 - \phi) \cdot h_b$. The parameter ϕ was tuned to give reasonable Deuterium-excess values and was subsequently set to 0.9.

[98] Equation (A1), together with mass conservation for both water and isotopes in the droplet, yields an equation for the evolution of the composition of the droplet [*Stewart*, 1975],

$$\frac{dR_l}{dm} = \beta \frac{R_l - \gamma R_b}{m}, \tag{A2}$$

with

$$\beta = \frac{1-\alpha\left(1-h_{eff}\right)\left(\frac{D}{D'}\right)^n}{\alpha(1-h_{eff})\left(\frac{D}{D}\right)^n}$$
$$\gamma = \frac{\alpha h_{eff}}{1-\alpha\left(1-h_{eff}\right)\left(\frac{D}{D'}\right)^n},$$

and where m is the raindrop mass.

[99] Although *Stewart* [1975] integrated this equation directly assuming that R_b was constant, we combine equation (A1) and mass conservation for the water and isotopes in the vapor of the unsaturated downdraft to yield the following equation for R_b:

$$\frac{dR_b}{dm} = A \frac{-R_l \cdot (1+\beta) + R_b \cdot (1+\beta\gamma).}{q^i_{p0} - A \cdot (m - m_0)}, \tag{A3}$$

with

$$A = \frac{w^i_t}{\Delta P \cdot \tilde{M}_p},$$

where w^i_t in the rain fall velocity, ΔP is the pressure difference between two levels. Here w^i_t and $\tilde{M}_p$ are assumed to be constant during the fractionating processes and m_0 is the initial raindrop mass.

[100] The equation system (A2) and (A3) is solved analytically and the following solution is obtained in the general case,

$$R_l = f^\beta g^{-\beta\gamma}\left(R_{l0}\left(1 + \gamma\beta\frac{A \cdot J}{q_{p0}}\right) + R_{b0}\gamma\beta\frac{J}{m_0}\right) \tag{A4}$$

$$R_b = R_{b0} g^{-1}\left(1 - f^{\beta+1} g^{-\beta\gamma}\gamma\beta\frac{A \cdot J}{q_{p0}}\right) + R_{l0} g^{-1}\frac{A \cdot m_0}{q_{p0}}\left(1 - f^{\beta+1} g^{-\beta\gamma}\left(1 + \gamma\beta\frac{A \cdot J}{q_{p0}}\right)\right), \tag{A5}$$

where $f(m) = \frac{m}{m_0}$, $g(m) = \frac{qp0 - A(m-m_0)}{q_{p0}}$, and $J = \int_m^{m_0} g(m')^{\beta\gamma-1} f(m')^{-(1+\beta)} dm'$. R_{l0} is the initial isotopic ratio of the raindrop, R_{b0} the initial isotopic ratio of the vapor of the unsaturated downdraft, f the residual fraction of rain droplet and g the increase of water vapor content in the unsaturated downdraft.

[101] Physically, the isotopic processes in the unsaturated downdraft depends on the relative humidity.

[102] 1. When the relative humidity h tends toward 1, there is virtually no reevaporation, and diffusive exchanges take place between the droplets and the downdraft vapor so as to drive the two phases toward isotopic equilibrium,

$$R_l \rightarrow \alpha_{eq} \cdot R_b$$

Typically, as rain falls into layers that are more and more enriched, diffusive exchanges tend to enrich the precipitation and deplete the vapor around it.

[103] 2. On the contrary, when h tends toward 0, there is no vapor for the raindrop to reequilibrate with. The reevaporation acts like a reverse Rayleigh distillation, with the raindrop getting more and more enriched as the reevaporation proceeds,

$$R_l = R_{l0} \cdot f^{\frac{\left(\frac{D}{D'}\right)}{\alpha} - 1}$$

The vapor also gets more and more enriched during the reevaporation process. Indeed, in the limit case where all the rain is reevaporated, the vapor composition is the weighted mean between the compositions of the original vapor and rain. This composition is richer than the original vapor composition since the condensate is always richer than the vapor.

[104] 3. For intermediate relative humidities, the processes are intermediate between a reverse Rayleigh distillation and an equilibration through diffusive exchanges. For high relative humidities, the diffusive exchanges dominate, whereas the "Rayleigh" reevaporation process dominates for low relative humidities.

Appendix B: Single-Column Simulations Using the Weak Temperature Gradient Approximation

[105] The thermodynamic equation used by the single column model to compute the temperature may be expressed as

$$\frac{\partial T}{\partial t} + \vec{V_H} \cdot \nabla T + \omega S = Q_{diabatic}, \tag{B1}$$

where $S = (T/\theta)\partial\theta/\partial p$ is the model static stability $\vec{V_H}$, ∇T is the horizontal temperature gradient ($\vec{V_H}$ is the horizontal wind), and $Q_{diabatic}$ is the sum of the convective, radiative and turbulent heating rates computed by the model parameterizations.

[106] Traditionally, SCM calculations are performed by specifying ω and then by predicting the temperature prognostically. In the approach using the Weak Temperature Gradient (WTG) approximation, the second left-hand-side term of the thermodynamic equation is neglected above the planetary boundary layer (at pressures below 800 hPa), the temperature profile of the free troposphere is specified (rather than predicted), and ω is calculated (rather than imposed) by the model physics and the assumption that the adiabatic cooling balances the diabatic heating [*Sobel and Bretherton*, 2000]: by fixing the vertical temperature profile above the boundary layer to an externally imposed profile, the vertical velocity ω may be diagnosed as: $\omega = Q_{diabatic}/S$.

[107] In this study, the temperature profile imposed (and fixed in time) above the boundary layer is derived from a radiative-convective equilibrium simulation performed with the same model, run in normal mode, for an SST of 29°C, a surface wind speed of 5 m/s, and no vertical velocity. Radiative-convective equilibrium simulations are then run in WTG mode for different SSTs ranging from 27°C to 29.8°C.

[108] Within the boundary layer (below the 800 hPa level), the temperature remains interactive and the vertical velocity is specified by vertical interpolation, by imposing that ω varies linearly with pressure between 800 hPa and the surface, and that $\omega = 0$ at the surface.

[109] **Acknowledgments.** We thank Jean-Yves Grandpeix, Georg Hoffmann, and Jean Jouzel for useful discussions about the physics of water stable isotopes or atmospheric convection. We are also grateful to Steven Sherwood for his thoughtful comments on an earlier version of this manuscript that helped us to improve the presentation of this study, and to Kerry A. Emanuel and Raymond T. Pierrehumbert for constructive reviews and suggestions. This work was funded by CNRS, by IPSL, and by the French national programs for climate studies (PNEDC-LEFE) Amancay and MISSTERRE.

References

Adler, R. F., et al. (2003), The Version 2 Global Precipitation Climatology Project (GPCP) monthly precipitation analysis (1979–present), *J. Hydrometeorol.*, *4*, 1147–1167.

Benedict, J. J., and D. A. Randall (2007), Observed characteristics of the MJO relative to maximum rainfall, *J. Atmos. Sci.*, *64*, 2332–2354.

Bergman, J. W., and P. D. Sardeshmukh (2004), Dynamic stabilization of atmospheric single column models, *J. Clim.*, *17*, 1004–1021.

Bony, S., and K. A. Emanuel (2001), A parameterization of the cloudiness associated with cumulus convection: Evaluation using TOGA COARE data, *J. Atmos. Sci.*, *58*, 3158–3183.

Bony, S., K.-M. Lau, and Y. C. Sud (1997), Sea surface temperature and large-scale circulation influences on tropical greenhouse effect and cloud radiative forcing., *J. Clim.*, *10*, 2055–2077.

Bony, S., J.-L. Dufresne, H. LeTreut, J.-J. Morcrette, and C. Senior (2004), On dynamic and thermodynamic components of cloud changes, *Clim. Dyn.*, *22*, 71–86.

Broecker, W. S. (1997), Mountain glaciers: Recorders of atmospheric water vapor content?, *Global Biogeochem. Cycles*, *11*, 589–598, doi:10.1029/97GB02267.

Cappa, C., M. Hendricks, D. DePaolo, and R. Cohen (2003), Isotopic fractionation of water during reevaporation, *J. Geophys. Res.*, *108*(D16), 4525, doi:10.1029/2003JD003597.

Chen, S. S., R. A. Houze Jr., and B. E. Mapes (1996), Multiscale variability of deep convection in relation to large-scale circulation in TOGA COARE, *J. Atmos. Sci.*, *53*, 1380–1409.

Chiang, J. C. H., and A. H. Sobel (2002), Tropical tropospheric temperature variations caused by ENSO and their influence on the remote tropical climate, *J. Clim.*, *15*, 2616–2631.

Cole, J. E., D. Rind, R. S. Webb, J. Jouzel, and R. Healy (1999), Climatic controls on interannual variability of precipitation $\delta^{18}O$: Simulated influence of temperature, precipitation amount, and vapor source region, *J. Geophys. Res.*, *104*, 14,223–14,236, doi:10.1029/1999JD900182.

Dansgaard, W. (1964), Stable isotopes in precipitation, *Tellus*, *16*, 436–468.

Dessler, A. E., and S. C. Sherwood (2003), A model of HDO in the tropical tropopause layer, *Atmos. Chem. Phys.*, *3*, 2173–2181.

Dessler, A. E., T. F. Hanisco, and S. Fueglistaler (2007), Effects of convective ice lofting on H_2O and HDO in the tropical tropopause layer, *J. Geophys. Res.*, *112*, D18309, doi:10.1029/2007JD008609.

Emanuel, K. A. (1991), A scheme for representing cumulus convection in large-scale models, *J. Atmos. Sci.*, *48*, 2313–2329.

Emanuel, K. A. (1997), Overview of atmospheric convection, in *The Physics and Parameterization of Moist Convective Atmospheric Convection*, edited by R. K. Smith, pp. 1–28, Kluwer Acad., Dordrecht, Netherlands.

Emanuel, K. A., and M. Zivkovic-Rothman (1999), Development and evaluation of a convection scheme for use in climate models, *J. Atmos. Sci.*, *56*, 1766–1782.

Emanuel, K. A., J. D. Neelin, and C. S. Bretherton (1994), On large-scale circulations in convecting atmospheres, *Q. J. R. Meteorol. Soc.*, *120*, 1111–1143.

Folkins, I., M. Loewenstein, J. Podolske, S. J. Oltmans, and M. Proffitt (1999), A 14 km mixing barrier in the tropics: Evidence from ozonesondes and aircraft measurements., *J. Geophys. Res.*, *104*, 22,095–22,102.

Fouquart, Y., and B. Bonnel (1980), Computation of solar heating of the Earth's atmosphere: A new parameterization, *Beitr. Phys. Atmos.*, *53*, 35–62.

Garreaud, R. D. (2000), Intraseasonal variability of moisture and rainfall over the South American Altiplano, *Mon. Weather Rev.*, *128*, 3346–3379.

Gat, J. R., and E. Matsui (1991), Atmospheric water balance in the Amazon basin: An isotopic evapotranspiration model, *J. Geophys. Res.*, *96*, 13,179–13,188.

Gettelman, A., and C. R. Webster (2005), Simulations of water isotope abundances in the upper troposphere and lower stratosphere and implications for stratosphere troposphere exchange, *J. Geophys. Res.*, *110*, D17301, doi:10.1029/2004JD004812.

Hanisco, T., et al. (2007), Observations of deep convective influence on stratospheric water vapor and its isotopic composition, *Geophys. Res. Lett.*, *34*, L04814, doi:10.1029/2006GL027899.

Hartmann, D. L., and M. L. Michelsen (1993), Large-scale effects on the regulation of tropical sea surface temperature, *J. Clim.*, *6*, 2049–2062.

Hartmann, D. L., J. R. Holton, and Q. Fu (2001), The heat balance of the tropical tropopause, cirrus, and stratospheric dehydration, *Geophys. Res. Lett.*, *28*, 1969–1972.

Hoffmann, G., M. Werner, and M. Heimann (1998), Water isotope module of the ECHAM atmospheric general circulation model: A study on time-

scales from days to several years, *J. Geophys. Res.*, *103*, 16,871–16,896, doi:10.1029/98JD00423.

Hoffmann, G., et al. (2003), Coherent isotope history of Andean ice cores over the last century, *Geophys. Res. Lett.*, *30*(4), 1179, doi:10.1029/2002GL014870.

Hourdin, F., et al. (2006), The LMDZ general circulation model: Climate performance and sensitivity to parameterized physics with emphasis on tropical convection, *Clim. Dyn.*, *19*(15), 3445–3482, doi:10.1007/s00382-006-0158-0.

Houze, R. A., Jr. (1981), Structures of atmospheric precipitation systems: A global survey, *Radio Sci.*, *16*, 671–689.

Johnson, D. G., K. W. Jucks, W. A. Traub, and K. V. Chance (2001), Isotopic composition of stratospheric water vapor: Implications for transport, *J. Geophys. Res.*, *106*, 12,219–12,226, doi:10.1029/2000JD900764.

Jouzel, J. (2003), Treatise on Geochemistry, vol. 4, *Water Stable Isotopes: Atmospheric Composition and Applications in Polar Ice Core Studies*, edited by R. F. Keeling, H. D. Holland, and K. K. Turekian pp. 213–243, Elsevier, New York.

Jouzel, J., and L. Merlivat (1984), Deuterium and oxygen 18 in precipitation: Modeling of the isotopic effects during snow formation, *J. Geophys. Res.*, *89*, 11,749–11,757.

Keith, D. W. (2000), Stratosphere-troposphere exchange: inferences from the isotopic composition of water vapor, *J. Geophys. Res.*, *105*, 15,167–15,173.

Kuang, Z., G. C. Toon, P. O. Wennberg, and Y. L. Yung (2003), Measured HDO/H_2O ratios across the tropical tropopause, *Geophys. Res. Lett.*, *30*(7), 1372, doi:10.1029/2003GL017023.

Küpper, C., J. Thuburn, G. C. Craig, and T. Birner (2004), Mass and water transport into the tropical stratosphere: A cloud-resolving simulation, *J. Geophys. Res.*, *109*, D10111, doi:10.1029/2004JD004541.

Lawrence, J. R., and S. D. Gedzelman (1996), Low stable isotope ratios of tropical cyclone rains, *Geophys. Res. Lett.*, *23*, 527–530, doi:10.1029/96GL00425.

Lawrence, J. R., S. D. Gedzelman, D. Dexheimer, H.-K. Cho, G. D. Carrie, R. Gasparini, C. R. Anderson, K. P. Bowman, and M. I. Biggerstaff (2004), Stable isotopic composition of water vapor in the tropics, *J. Geophys. Res.*, *109*, D06115, doi:10.1029/2003JD004046.

Lindzen, R. S., and S. Nigam (1987), On the role of sea surface temperature gradient in forcing low-level winds and convergence in the tropics, *J. Atmos. Sci.*, *44*, 2418–2431.

Majoube, M. (1971a), Fractionnement en oxygène 18 entre la glace et la vapeur d'eau, *J. Chim. Phys. Phys. Chim. Biol.*, *68*, 625–636.

Majoube, M. (1971b), Fractionnement en oxygène 18 et en deutérium entre l'eau et sa vapeur, *J. Chim. Phys. Phys. Chim. Biol.*, *68*, 1423–1436.

Mathieu, R., D. Pollard, J. Cole, J. W. C. White, R. S. Webb, and S. L. Thompson (2002), Simulation of stable water isotope variations by the GENESIS GCM for modern conditions, *J. Geophys. Res.*, *107*(D4), 4037, doi:10.1029/2001JD900255.

McGuffie, K., and A. Henderson-Sellers (2004), Stable water isotope characterization of human and natural impacts on land-atmosphere exchanges in the Amazon Basin, *J. Geophys. Res.*, *109*, D17104, doi:10.1029/2003JD004388.

Merlivat, L. (1978), Molecular diffusivitied of $H_2^{16}O$, $HD^{16}O$, and $H_2^{18}O$ in gases, *J. Chem. Phys.*, *69*, 2864–2871.

Merlivat, L., and J. Jouzel (1979), Global climatic interpretation of the deuterium-oxygen 18 relationship for precipitation, *J. Geophys. Res.*, *84*, 5029–5032.

Merlivat, L., and G. Nief (1967), Fractionnement isotopique lors des changements d'états solide-vapeur et liquide-vapeur de l'eau des températures inférieures à 0°C, *Tellus*, *19*, 122–127.

Morcrette, J.-J. (1991), Radiation and cloud radiative propertied in the european centre for medium-range weather forecasts forecasting system, *J. Geophys. Res.*, *96*, 9121–9132.

Moyer, E. J., F. W. Irion, Y. L. Yung, and M. R. Gunson (1996), ATMOS stratospheric deuterated water and implications for troposphere-stratosphere transport, *Geophys. Res. Lett.*, *23*, 2385–2388, doi:10.1029/96GL01489.

Nassar, R., P. F. Bernath, C. D. Boone, A. Gettelman, S. D. McLeod, and C. P. Rinsland (2007), Variability in HDO/H_2O abundance ratios in the tropical tropopause layer, *J. Geophys. Res.*, *112*, D21305, doi:10.1029/2007JD008417.

New, M., M. Hulme, and P. D. Jones (1999), Representing twentieth century space-time climate variability. Part 1: Development of a 1961–90 mean monthly terrestrial climatology, *J. Clim.*, *12*, 829–856.

Newell, R. E., and S. Gould-Stewart (1981), A stratospheric fountain?, *J. Atmos. Sci.*, *38*, 2789–2796.

Noone, D., and I. Simmonds (2002), Associations between $\delta^{18}O$ of water and climate parameters in a simulation of atmospheric circulation for 1979–95, *J. Clim.*, *15*, 3150–3169.

Pierrehumbert, R. T. (1999), Huascaran $\delta^{18}O$ as an indicator of tropical climate during the Last Glacial Maximum, *Geophys. Res. Lett.*, *26*, 1345–1348, doi:10.1029/1999GL900183.

Ramirez, E., et al. (2003), A new Andean deep ice core from Nevado Illimani (6350 m), Bolivia, *Earth Planet. Sci. Lett.*, *212*, 337–350.

Raymond, D. J., and A. M. Blyth (1986), A stochastic model for nonprecipitating cumulus clouds, *J. Atmos. Sci.*, *43*, 2708–2718.

Reynolds, R. W., N. A. Rayner, T. M. Smith, D. C. Stokes, and W. Wang (2002), An improved in situ and satellite SST analysis for climate, *J. Clim.*, *15*, 1609–1625.

Risi, C., S. Bony, and F. Vimeux (2008), Influence of convective processes on the isotopic composition ($\delta^{18}O$ and δD) of precipitation and atmospheric water in the tropics: 2. Physical interpretation of the amount effect, *J. Geophys. Res.*, *113*, D19306, doi:10.1029/2008JD009943.

Rosenlof, K. H. (2003), How water enters the stratosphere, *Science*, *302*, 1691–1692.

Rozanski, K., L. Araguás-Araguás, and R. Gonfiantini (1993), Isotopic patterns in modern global precipitation, in *Climate Change in Continental Isotopic Records, Geophys. Monogr. Ser.*, vol. 78, edited by P. K. Swart et. al., pp. 1–36, AGU, Washington, D. C.

Schmidt, G., G. Hoffmann, D. Shindell, and Y. Hu (2005), Modelling atmospheric stable water isotopes and the potential for constraining cloud processes and stratosphere-troposphere water exchange, *J. Geophys. Res.*, *110*, D21314, doi:10.1029/2005JD005790.

Sherwood, S. C., and A. E. Dessler (2001), A model for transport across the tropical tropopause, *J. Atmos. Sci.*, *58*, 765–779.

Sherwood, S. C., and C. L. Meyer (2006), The general circulation and robust relative humidity, *J. Clim.*, *19*, 6278–6290.

Smith, J. A., A. S. Ackerman, E. J. Jensen, and O. B. Toon (2006), Role of deep convection in establishing the isotopic composition of water vapor in the tropical transition layer, *Geophys. Res. Lett.*, *33*, L06812, doi:10.1029/2005GL024078.

Sobel, A. H., and C. S. Bretherton (2000), Modeling tropical precipitation in a single column, *J. Clim.*, *13*, 4378–4392.

Stewart, M. K. (1975), Stable isotope fractionation due to evaporation and isotopic exchange of falling waterdrops: Applications to atmospheric processes and evaporation of lakes, *J. Geophys. Res.*, *80*, 1133–1146.

Taylor, G. R., and M. B. Baker (1991), Entrainment and detrainment in cumulus clouds., *J. Atmos. Sci.*, *48*, 112–121.

Thompson, L. G., E. Mosley-Thompson, and K. A. Henderson (2000), Ice-core paleoclimate records in tropical south america since the Last Glacial Maximum, *J. Quat. Sci.*, *15*, 1579–1600.

Tompkins, A. M., and K. A. Emanuel (2000), The vertical resolution sensitivity of simulated equilibrium temperature and water vapour profiles, *Q. J. R. Meteorol. Soc.*, *126*, 1219–1238.

Uppala, S., et al. (2005), The ERA-40 re-analysis, *Q. J. R. Meteorol. Soc.*, *131*, 2961–3012.

Vimeux, F., R. Gallaire, S. Bony, G. Hoffmann, and J. C. H. Chiang (2005), What are the climate controls on δD in precipitation in the Zongo Valley (Bolivia)? Implications for the Illimani ice core interpretation, *Earth Planet. Sci. Lett.*, *240*, 205–220, doi:10.1016/j.epsl.2005.09.031.

Vuille, M., and M. Werner (2005), Stable isotopes in precipitation recording South American summer monsoon and ENSO variability: Observations and model results, *Clim. Dyn.*, *25*, 401–413, doi:10.1007/s00382-005-0049-9.

Vuille, M., R. S. Bradley, M. Werner, R. Healy, and F. Keimig (2003), Modeling $\delta^{18}O$ in precipitation over the tropical Americas: 1. Interannual variability and climatic controls, *J. Geophys. Res.*, *108*(D6), 4174, doi:10.1029/2001JD002038.

Webster, C. R., and A. J. Heymsfield (2003), Water isotope ratios D/H, $^{18}O/^{16}O$, $^{17}O/^{16}O$ in and out of clouds map dehydration pathways, *Science*, *302*, 1742–1746, doi:10.1126/science.1089496.

Worden, J., D. Noone, and K. Bowman (2007), Importance of rain evaporation and continental convection in the tropical water cycle, *Nature*, *445*, 528–532.

Xu, K.-M., and K. Emanuel (1989), Is the tropical atmosphere conditionally unstable?, *Mon. Weather Rev.*, *117*, 1471–1479.

Yanai, M., B. Chen, and W.-W. Tung (2000), The Madden-Julian Oscillation observed during the TOGA COARE IOP: Global view, *J. Atmos. Sci.*, *57*, 2374–2396.

S. Bony and C. Risi, Laboratoire de Météorologie Dynamique, IPSL, UPMC, CNRS, case courrier 99, 4 Place Jussieu, F-75252 Paris CEDEX 05, France. (bony@lmd.jussieu.fr)

F. Vimeux, IRD-UR Great Ice, LSCE, IPSL, CEA, UVSQ, CNRS, CE Saclay, Orme des Merisiers, Bât 701, F-91191 Gif-sur-Yvette CEDEX, France.